Ore Geology Reviews 76 (2016) 122–139

Contents lists available at ScienceDirect

Ore Geology Reviews

journal homepage: www.elsevier.com/locate/oregeorev

# Evidence for SEDEX-style mineralization in the 1.7 Ga Tawallah Group, McArthur Basin, Australia

Samuel C. Spinks [a,*], Susanne Schmid [a], Anais Pagés [a], Josh Bluett [b]

[a] CSIRO Mineral Resources, Australian Resources Research Centre, 26 Dick Perry Avenue, Kensington, WA 6151, Australia
[b] Armour Energy Limited, Level 27, 111 Eagle Street, Brisbane, QLD 4000, Australia

ARTICLE INFO

*Article history:*
Received 30 August 2015
Received in revised form 21 January 2016
Accepted 21 January 2016
Available online 22 January 2016

*Keywords:*
SEDEX
Base metals
Sedimentary deposits
McArthur Basin
Tawallah Group

ABSTRACT

The Paleoproterozoic McArthur Basin (McArthur Group) of northern Australia hosts world-class sedimentary 'exhalative' (SEDEX) McArthur type Zn–Pb deposits, which are largely hosted within a sequence of 1.64 Ga pyritic carbonaceous shales deposited in an extensional rift setting. A well-known example of these is McArthur River (or Here's Your Chance [HYC] Zn–Pb–Ag deposit). The ~1.78 Ga McDermott and ~1.73 Ga Wollogorang formations (Tawallah Group) both contain carbonaceous shales deposited in similar environments. Our observations suggest the carbonaceous facies of the Wollogorang Formation were deposited under mostly euxinic conditions, with periodically-high concentrations of sedimentary pyrite deposition. The carbonaceous shales in the older McDermott Formation contain considerably less early pyrite, reflecting a mostly sulfide-poor, anoxic depositional environment. Localized fault-bound sub-basins likely facilitated lateral facies variations, which is evident from synsedimentary breccias.

The presence of evaporitic oxidized facies within the McDermott and Wollogorang formations, alongside evidence for synsedimentary brecciation in reduced shales are favourable criteria for SEDEX-style base metal deposition. Both formations overlie volcanic units, which could have been sources of base metals. Detailed X-ray petrography, new geochemical data and sulfur isotope data from historical drill cores indicate multiple horizons of stratiform and sediment breccia-hosted base metal sulfide within carbonaceous shale units, with high-grade Zn concentrations. A close association between sphalerite and ferromanganean dolomite alteration draws comparisons with younger SEDEX mineralization at HYC. Additionally, SEDEX alteration indices, used demonstrably as a vector to the younger orebodies, indicate the sedimentary rocks analyzed in this study are marginally below the ore window when compared to the overlying mineralized stratigraphy.

Our data imply that localized active circulation of metalliferous brines occurred in the Tawallah Group basin. High-grade sulfide deposition in reduced facies alteration may represent distal expressions of larger SEDEX-style deposits. Furthermore, abundant pyrite and high molybdenum in the Wollogorang Formation suggest the global oceanic sulfate concentration was sufficient by ~1.73 Ga to engender intermittent but strong bottom-water euxinia during shale deposition, thus providing a robust chemical trap for base metal sulfide mineralization.



## 1. Introduction

### 1.1. Proterozoic sedimentary exhalative (SEDEX) base metal deposits

Stratiform 'sedimentary exhalative' (SEDEX) ore deposits are major sources of base metals such as Zn–Pb–Ag ± Cu–N–Mo–Ba (Li and Xi, 2015 and references therein) and are the primary sources of Zn and Pb (Large et al., 2005). The McArthur and neighbouring Isa basins of northern Australia host numerous SEDEX deposits. The main characteristics of SEDEX deposits in the McArthur-Isa basins are, as summarised in Large et al. (2005): laminated sphalerite and galena-bearing dolomitic siltstones; stacked ore lenses separated by carbonaceous mudstones; ore deposition adjacent to major faults; Fe–Mn dolomite alteration haloes; and no obvious vent or stringer zones. A generalised genetic model for deposition is of synsedimentary base metal sulfide precipitation facilitated by exhalation of metallic basinal brines from active fault zones (Large et al., 1998; 2000 Large and McGoldrick, 2000; Large et al., 2005), or by syndiagenetic replacement of carbonate (Large et al., 1998; Ireland et al., 2004). Two distinct categories of SEDEX deposits were proposed by Cooke et al. (2000) based on the mineralizing brines, sedimentary basin and lithology type: McArthur type (oxidized brines) and Selwyn type (reduced brines). SEDEX deposits of

* Corresponding author.
*E-mail address:* sam.spinks@csiro.au (S.C. Spinks).

http://dx.doi.org/10.1016/j.oregeorev.2016.01.007
0169-1368/

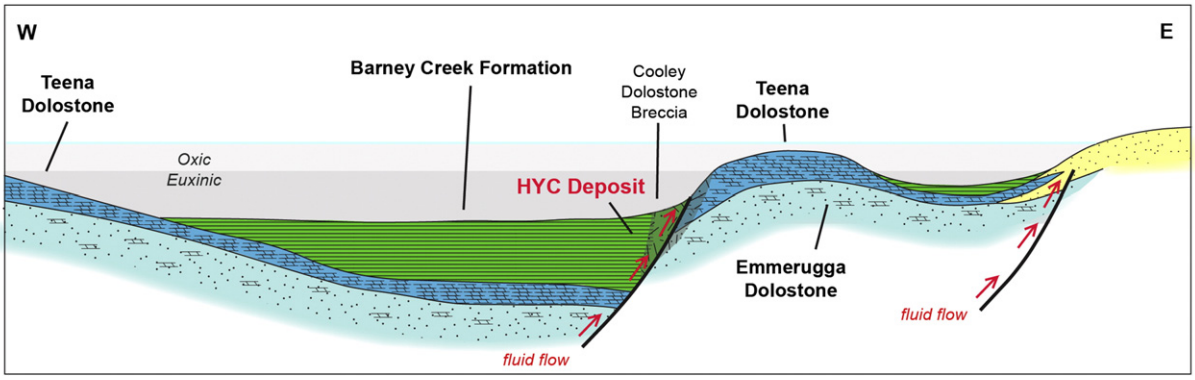


**Fig. 1.** Genetic model cross section of synsedimentary McArthur Type base metal sulfide SEDEX deposits, based on the geology of HYC (e.g. Large et al., 1998). 

the McArthur-type typically form by the following stages (Large et al., 1998; Large and McGoldrick, 2000; Cooke et al., 2000; Fig. 1):

1. Oxidizing brines descend from surface evaporitic environments into porous and fractured basin aquifers.
2. Basinal brines leach metals from underlying volcanics.
3. Sulfate-metal-bearing oxidized brines are released along fault zones into anoxic/euxinic basin floor or shallow subsurface.
4. Base metal sulfide precipitation through bacterial sulfate reduction or by interaction with biogenic $H_2S$.

The major known SEDEX deposits in the McArthur Basin (Fig. 2) occur within the Barney Creek Formation of the McArthur Group (Glyde Package; Figs. 1, 3) such as the McArthur River (or Here's Your Chance [HYC]) Zn–Pb–Ag deposit (Large et al., 1998; Large and McGoldrick, 2000). The volcanic and oxidized clastic lithologies

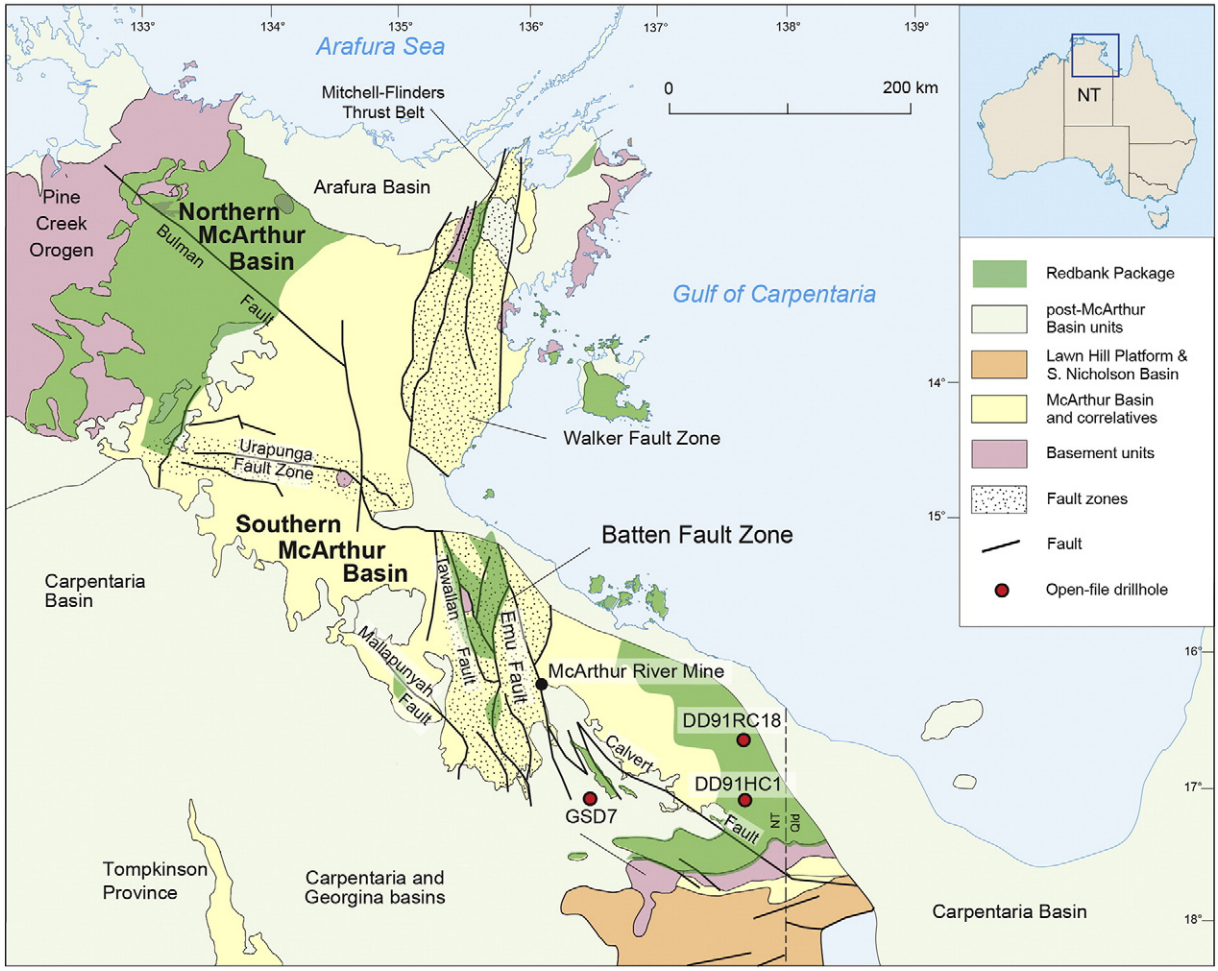


**Fig. 2.** Simplified geological map of the McArthur Basin of Northern Australia (modified after Ahmad et al., 2013 and references therein). 

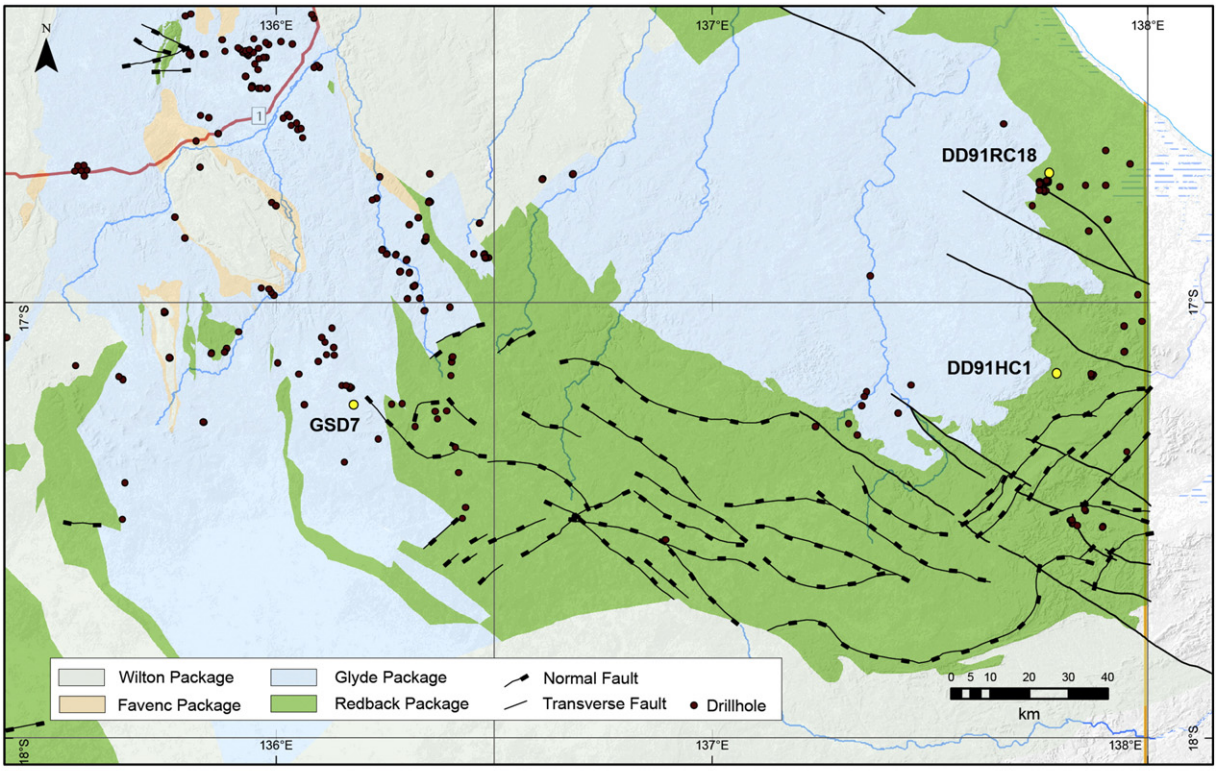


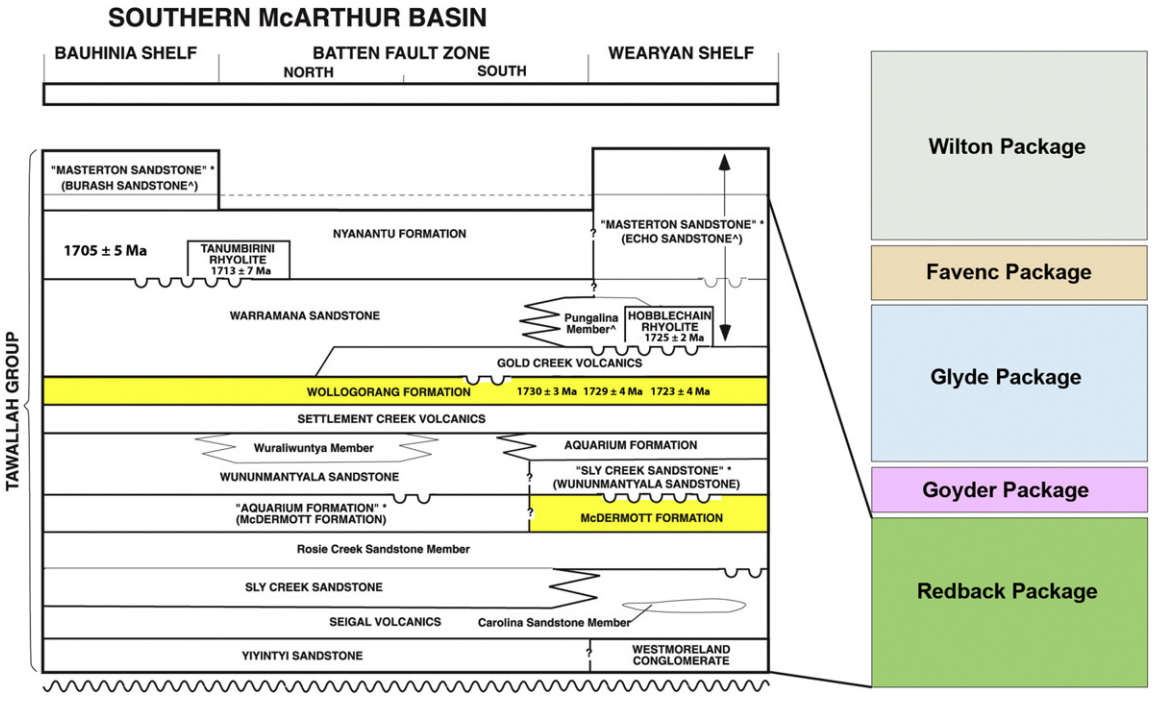


**Fig. 3.** Top: Detailed geological map of study area showing the collar locations of drillholes used in this study, and major structures. Bottom: Stratigraphic framework of the southern McArthur Basin showing subdivisions by group and 'packages' (modified from Rawlings (1999). 

underlying the Barney Creek Formation are thought to have been critical in the formation of the oxidized metal-rich brines that formed HYC and other prospects (Cooke et al., 2000), making the Barney Creek Formation the highest priority ongoing exploration target. However, recent exploration attention has also been focused on the shale-bearing stratigraphies of the Tawallah Group such as the McDermott and Wollogorang formations, as they also overlie volcanic and oxidized clastic facies and contain pyritic carbonaceous shale. These formations are underexplored and understudied, thus they are the subject of this study.

### *1.2. Geological setting*

#### *1.2.1. McArthur Basin*

The McArthur Basin in northern Australia is a spatially-extensive intracratonic Paleoproterozoic–Mesoproterozoic (1850–1450 Ma)

succession 5–15 km in depth. The basin consists of mostly non-metamorphosed marine and fluvial sediments and intercalated volcanics (Plumb, 1979; Rawlings, 1999; Ahmad et al., 2013). Overlying the metamorphosed Paleoproterozoic Pine Creek Orogen, the McArthur Basin is exposed over more than 180,000 km$^2$ in NE Northern Territory and extends toward the Isa Superbasin in northern Queensland. It is overlain by the Neoproterozoic Georgina and Cretaceous Carpentaria basins to the south (Fig. 2; Ahmad et al., 2013). The McArthur Basin is separated stratigraphically into the northern and southern McArthur Basin, which are divided by the Urupunga Fault Zone (Fig. 2). The stratigraphy in the northern McArthur Basin is divided into the Groote Eylandt, Katherine River, Donydji, Parsons Range, Habgood, Balma, Mount Rigg, Nathan and Roper groups (Fig. 3). In the south, the stratigraphy comprises the Tawallah, McArthur, Nathan, and Roper groups (Rawlings, 1999; Ahmad et al., 2013; Fig. 3**)**. The stratigraphy is further categorized into simplified 'packages', which in the southern McArthur Basin comprise the Redbank (Tawallah Group), Glyde (McArthur Group), Favenc (Nathan Group), and Wilton (Roper Group) packages (Fig. 3; Rawlings, 1999). A detailed account of the McArthur Basin is provided by Ahmed et al. (2013).

*1.2.2. Tawallah Group*

The Tawallah Group of the Redbank Package is the lowermost and oldest stratigraphic unit of the southern McArthur Basin. It is mostly exposed southeast of the Batten Fault Zone (Fig. 2). Deposited between ~1850 and ~1715 Ma, the Tawallah Group overlies basement volcanic units and is composed of basal conglomerate, basalts, varying shallow marine facies, fluvial and lacustrine facies, and basaltic and intrusive units. Within the marine sedimentary units, the McDermott and Wollogorang formations contain organic-rich mudstone and carbonate facies, potentially favourable for McArthur type SEDEX mineralization (Fig. 3). Neither formation is thus far known to be significantly mineralized with base metals, but enrichments in Zn, Pb, and Cu have been identified at several stratigraphic levels (Jackson, 1985; Donnelly and Jackson, 1988; Kendall et al., 2009).

The McDermott Formation is the oldest mudstone-bearing sedimentary unit within the Tawallah Group. It overlies the Seigal Volcanics and is overlain by the Sly Creek Sandstone (Jackson et al., 1987, Fig. 3). Accurate depositional ages for the McDermott Formation are not currently available, but an approximate age for deposition is derived from the maximum to minimum age of 1780 to 1760 Ma of the conformably underlying Seigal Volcanics (Rawlings, 1999). The sedimentary succession consists of basal sandstone, interbedded carbonaceous siltstone and stromatolitic dolostone, and upper fluvial sandstones and red mudstones (Figs. 4, 5).

The Wollogorang Formation is a laterally-extensive but relatively thin shallow marine to near-shore clastic sedimentary unit with a maximum thickness of around 150 m (Jackson, 1985). It is both underlain and overlain by extrusive and intrusive volcanic units, and has a depositional age between 1730 ± 3 and 1729 ± 4 Ma from tuffaceous green clays (Page et al., 2000). The sedimentary sequence consists of red brown dolomitic mudstone with stromatolites, evaporites, and carbonaceous grey dolostone; dolomitic black carbonaceous siltstone; and the youngest dolomitic sandstone and quartz sandstone with minor dololutite. A key marker horizon in the Wollogorang Formation is the presence of round diagenetic dolomitic nodules within black carbonaceous mudstone close to the base of the sequence (Figs. 6, 7).

*1.3. Sedimentology and alteration*

*1.3.1. McDermott formation*

The sedimentary succession in drill hole GSD7 (Figs. 2, 3, 4) consists of grey dolomitic mudstone and dolostone/limestone. The dolomitic siltstone is well-laminated with gypsum pseudomorphs, chert nodules, bituminous staining and stromatolites. The dolostone/limestone contains stromatolites and bituminous staining, carbonate breccias with limestone/dolostone, bituminous stylolites, carbonate nodules, gypsum pseudomorphs, and needle-shaped pseudomorphs of evaporite minerals. The upper section is characterized by fining upward cycles of coarse grained sandstone grading to dark red to green mudstone. The drill hole terminated within black shale facies.

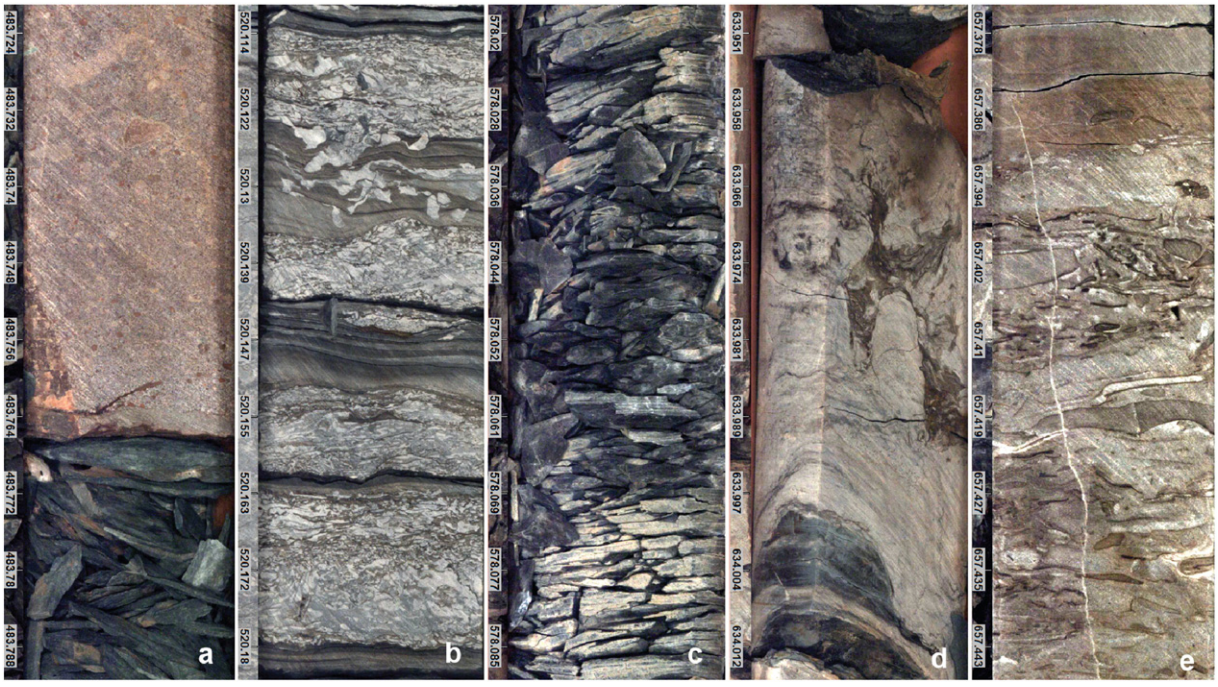


**Fig. 4.** Core photographs of GSD7 (McDermott Formation) showing a: upper core intervals with sharp contact of dark grey siltstone and shale and red fluvial, coarse grained sandstone (from 483.7 m); b: thinly laminated, dolomitic and calcareous siltstone with abundant gypsum pseudomorphs (from 520.1 m); c: typical (poorly preserved) dark grey shale (from 578.0 m); d: stromatolites within a thick dolostone interval (from 633.9 m); and e: abundant algal mats fragments with bituminous coating in a thick dolostone interval (from 657.3 m). 

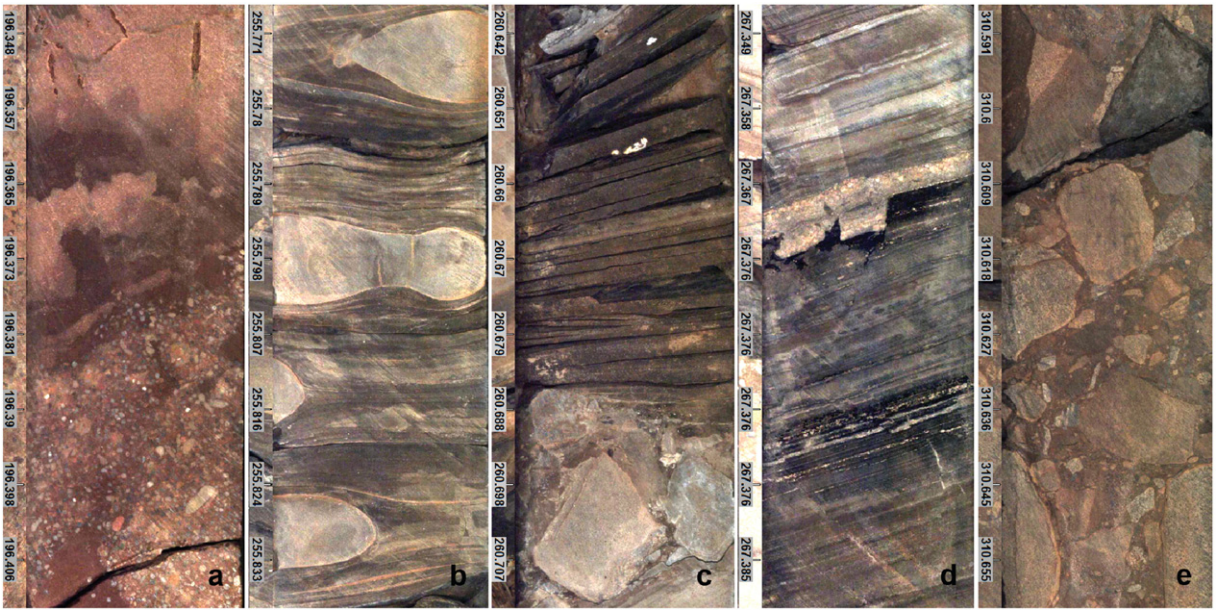


**Fig. 5.** Core imagery of the Wollogorang Formation from DD91RC18 showing a: red coarse grained to fine grained sandstone in the upper part of the succession (from 195.3 m), b: characteristic carbonate nodules within laminated calcareous and dolomitic siltstone and shale (from 255.7 m), c: intraformational breccia overlain by laminated siltstone and shale (from 260.6 m), d: bituminous staining along microfractures in finely laminated dolostone and siltstone (from 267.3 m), and e: basal carbonate breccia in contact to the underlying volcanic succession (from 310.5 m). 

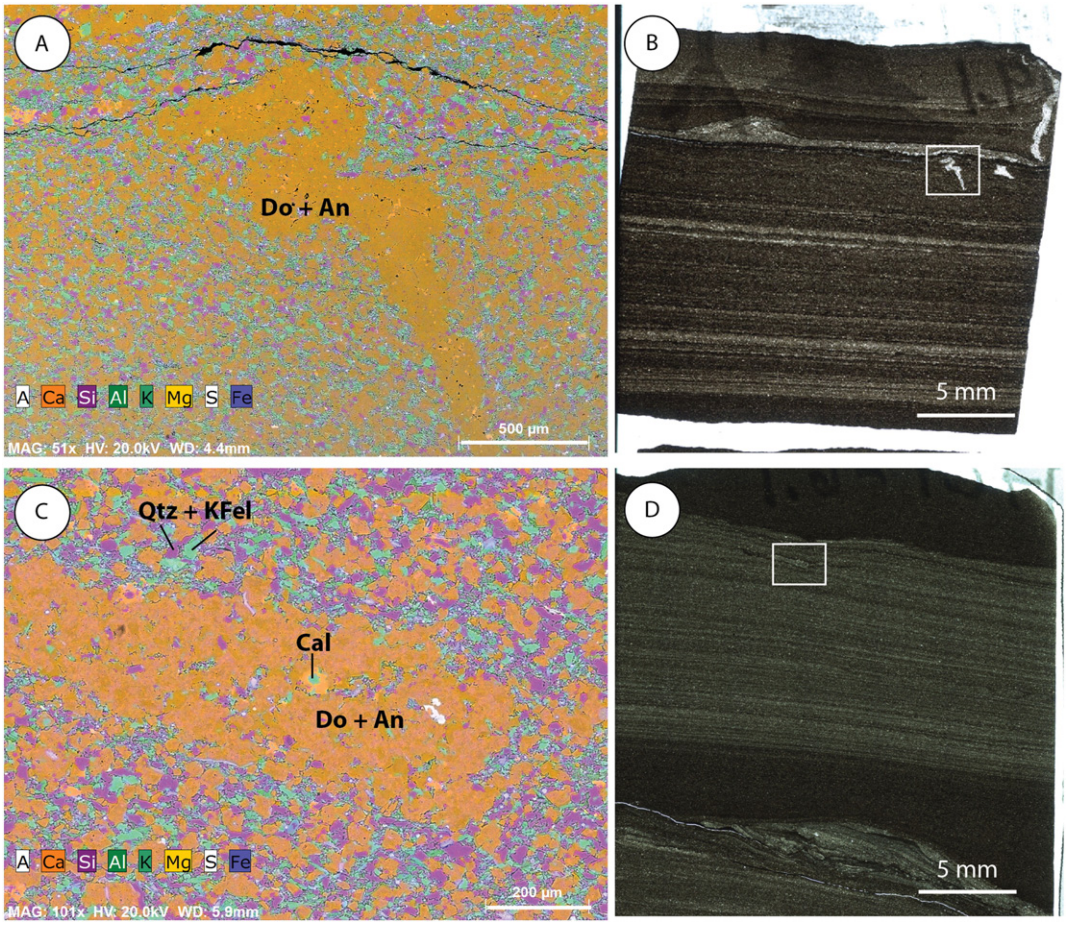


**Fig. 6.** Wollogorang Formation Mn–Fe dolomite (ankerite) alteration montage (DD91HC1–284.6 m). A, C) FEG-SEM element map of dolomite/ankerite alteration in siltstone and synaeresis crack (DD91HC1–284.6 and 273.6 m). Qtz = Quartz, K Fel = K feldspar, Dol = Dolomite, Ank = Ankerite, Cal = Calcite. B, D) Corresponding thin section micrographs showing fields of view in A, C. 

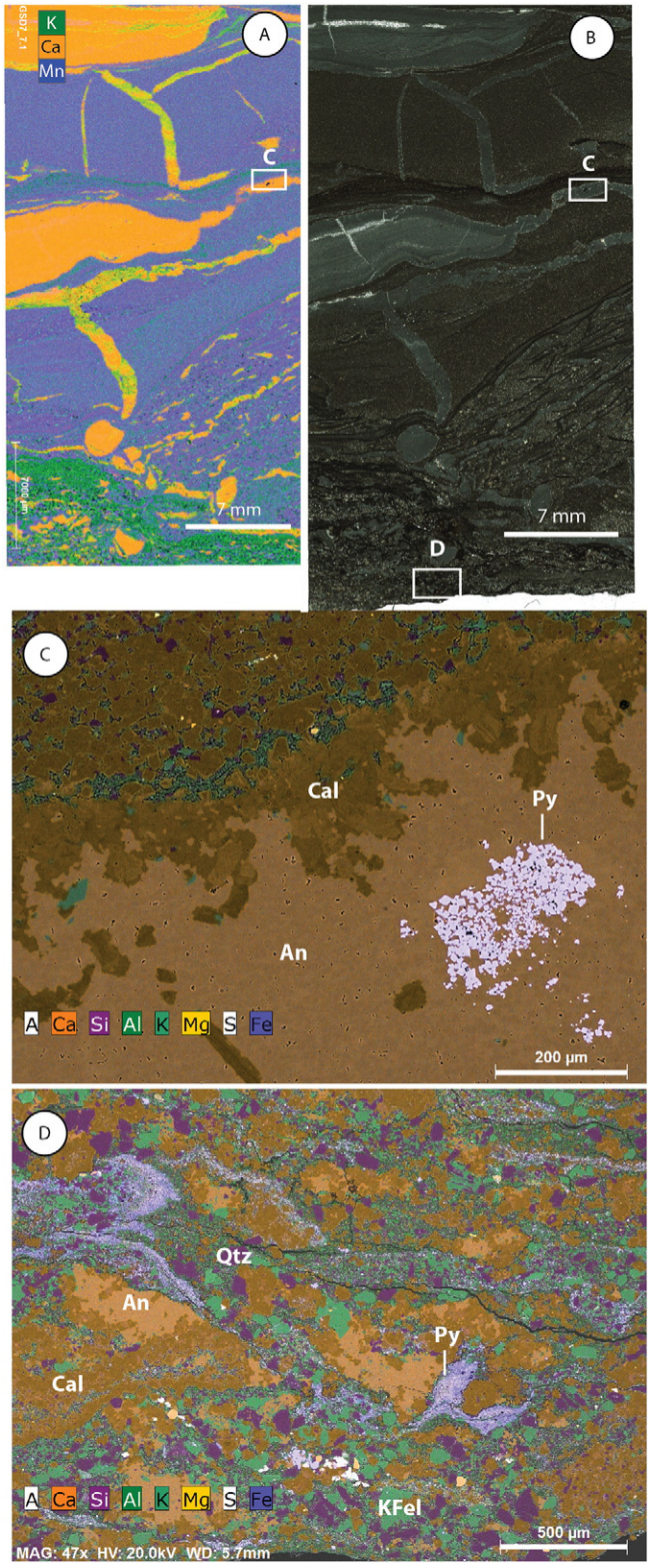


**Fig. 7.** Potassic alteration montage. A) XFR map of section from GSD7 530.6 m showing areas of ankerite (blue), calcite nodules (orange) and alteration-feldspar associated with hydrocarbons (green). B) Transmitted light micrograph of field of view in A. C) FEG-SEM element map of ankerite and calcite with associated pyrite Ank = Ankerite, Cal = Calcite, Py = Pyrite. D) FEG-SEM element map of zone of potassic alteration (green) with associated hydrocarbon flows, as is evident by flow fronts of pyrite. Qtz = Quartz, K Fel = K feldspar, Dol = Dolomite, Ank = Ankerite, Cal = Calcite, Py = Pyrite. 

The McDermott Formation is interpreted to have been deposited within a shallow marine evaporitic environment, indicated by gypsum pseudomorphs and evaporite needles. An intraformational breccia, carbonate nodules and thin tuff beds intersected at depths between 649 and 663 m imply a change in depositional settings, with potential deepening of the basin. The lithologies from 649 to 610 m are dominantly carbonates and siliciclastic carbonates containing stromatolites. They are interpreted to have been deposited in a shallow marine to carbonate platform environment. The succession from 618 to 484 m contains a mixture of debris flows, pisolitic limestone, stromatolites and gypsum pseudomorphs, all indicating a shallow marine to evaporitic conditions. The lithologies from 484 to 421 m show increasing sand content and minor fluvial channels and are interpreted to be deposited in shallow marine to coastal settings. Thick medium-grained sandstone intervals with reworked mudstone tops from 421 to 377 m implies fluvial input into the basin. The interval between 377 and 350 m is dominated by red mudstones with a sandstone base, with 10–20 m thick fining upward cycles with minor debris flows interpreted to be deposited in a shallow marine to restricted, potentially lacustrine environment. The sandstones above 350 m are similar to the sandstone succession below 377 m and are interpreted to be of fluvial origin. Overall the sequence is interpreted to have been deposited during sea level regression from deep anoxic deposition, shoreline lacustrine sediments in the middle section and increasing clastic sediment input from the hinterland in the upper section.

### *1.3.2. Wollogorang formation*

Paleoproterozoic Wollogorang Fm. sedimentary facies in drill holes DD91RC18 and DD91HC1 (Figs. 2, 3) are underlain by basaltic Settlement Creek Volcanics and overlain by the Gold Creek Volcanics (Fig. 3). The sedimentary succession between two volcanic units is largely characterized by fining upward cycles of thin basal sandstone and thick red mudstone with minor brecciated beds, greenish brown thick cherty mudstone, brecciated cherty mudstone with stromatolites, and grey mudstone interbedded with siltstone containing carbonate nodules. The characteristic carbonate nodules are bituminous and brecciated in parts. The basal contact with the Settlement Creek Volcanics consists of a breccia containing volcanic and sedimentary clasts.

The basal sedimentary rocks are interpreted to have been deposited within a shallow evaporitic environment which gradually deepened, facilitating the deposition of muddy organic-rich facies. The uppermost sandstones were deposited in a fluvially-dominated system in either a near-shore marine or terrestrial environment.

Intraformational brecciation within the muddy shale facies is characterized by rectangular black shale and minor light grey carbonate clasts within massive black muddy matrix. Individual shale clasts within the brecciated zone commonly contain bitumen clasts and evidence for migrated hydrocarbon flows such as bitumen-filled soft sediment deformation structures observed within the matrix, imply significant hydrocarbon generation within the basin. Brecciation of the shales is interpreted to have been synsedimentary, with older hydrocarbon-bearing compacted shale and carbonate clasts emplaced during slump events.

### *1.3.3. Alteration and diagenesis*

Dolomite alteration with varying Mn–Fe (ankerite) concentrations occurs throughout the studied sections of the Wollogorang and McDermott formations (Fig. 6). Intensities and degrees of alteration vary, but clastic silty facies in drill holes DD91RC18 and GSD7 commonly display almost complete dolomitic alteration with associated sulfides such as sphalerite. In both formations, laminated carbonaceous siltstone with coarser laminae of primary authigenic carbonate occur throughout the fine grained facies units. The carbonate laminae display almost total dolomite alteration, that is locally ferroan to ankeritic in composition, with very little original calcite remaining. This is illustrated in Fig. 6, which shows both carbonate-filled synaeresis cracks and depositional

carbonate laminae which have undergone dolomite alteration. It is within these altered laminae where most of the sphalerite mineralization is observed (see Sections 3, 4).

Additionally, potassic alteration occurs locally in the McDermott Formation, apparently in association with hydrocarbon migration. Fig. 7 shows a section of nodular calcite which has undergone partial dolomite (ankerite) alteration of the fine grained matrix and lensoid-shaped nodules and crack fills. The lower part of the section of Fig. 7A (Fig. 7D) shows localised brecciation with flows of hydrocarbons indicated in the element map by pyritic flow fronts. This area has undergone later K-feldspar alteration of quartzofeldspathic clastic grains, and carbonaceous muds. The K-feldspar alteration of this zone overprints earlier dolomite alteration (Fig. 7D).

Siliciclastic silt laminae within the shale units of the Wollogorang and McDermott formations have undergone quartzofeldspathic and carbonate diagenetic cementation. Fig. 8 shows fine-grained pyritic carbonaceous mud laminae interbedded with coarser-grained silt laminae. The silt laminae are composed of quartz and K-feldspar grains with authigenic calcite, and minor micas and clays. All three mineral phases have been subject to overgrowths of similar compositions, resulting in interlocked crystal contacts and decreased porosity.

## 2. Methods and materials

### 2.1. Sampling

This study focused on three open-access stratigraphic diamond drill cores located at the Northern Territory Geological Survey Core Library in Darwin, Australia: DD91RC18, DD91HC1 and GSD7 (Figs. 2, 3). All three holes were drilled in the 1990s by CRA Exploration Pty. (DD91HC1 and DD91RC18) and BHP Minerals Pty. Ltd. (GSD7) during exploration for hydrocarbons and minerals within the McArthur Basin. Samples were selected from core at regular intervals for multi-element geochemical analysis and petrography, and macroscopic sulfide-bearing sections were sampled for sulfur isotope analyses. Whole-rock splits, sulfide grains, and polished thin sections were prepared at CSIRO's sample preparation facility in Perth, Western Australia.

### 2.2. Multi-element geochemistry

Multi-element assay on whole-rock pulps was performed at ACME Analytical Labs in Canada using a multi-acid ($HNO_3$–$HClO_4$–HF–HCl) digest, and ICP-ES/MS analysis. Elements analysed were Ag, Al, As, Ba, Be, Bi, Ca, Cd, Ce, Co, Cr, Cs, Cu, Dy, Eu, Fe, Ga, Gd, Hf, Ho, In, K, La, Li, Lu, Mg, Mn, Mo, Na, Nb, Nd, Ni, P, Pb, Pr, Rb, Re, S, Sb, Sc, Se, Sm, Sn, Sr, Ta, Tb, Te, Th, Ti, Tl, Tm, U, V, W, Y, Yb, Zn, Zr. Major oxides, including $SiO_2$, $Al_2O_3$, $Fe_2O_3$, CaO, MgO, $Na_2O$, $K_2O$, MnO, $TiO_2$, $P_2O_5$, $Cr_2O_3$ and Ba, were analysed by XRF. Additionally, total carbon (TC) and total sulfur (TS) were analysed by a Leco Infrared Carbon–Sulfur analyser.

Total organic carbon (TOC) was measured at LabWest Minerals Analysis Pty Ltd. in Perth, WA. Pulped samples were digested in 20% HCl for 24 h to remove authigenic and diagenetic carbonate, then twice rinsed with distilled water. Dried pulps were then analysed using a Leco Infrared Carbon analyser.

Additional analysis of samples which returned Zn concentrations above detection limit (>1%) was performed using an Innovex 40 kV Portable XRF. Full data are available in Supplementary Table 2.

#### 2.2.1. Data treatment

ACME Analytical Labs performed duplicate analyses on 7 samples for 4-acid ICP-ES/MS multi-element, major oxide XRF, and TC/TS Leco

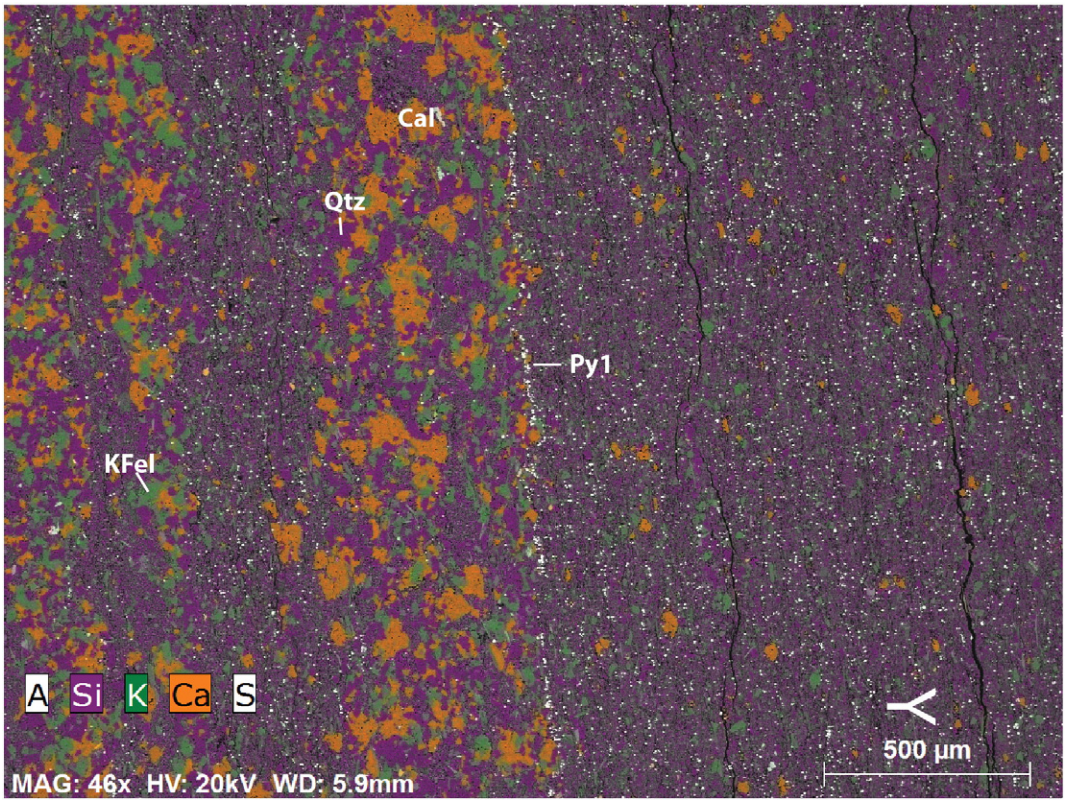


**Fig. 8.** FEG-SEM element map of typical sulfidic organic matter-rich and coarse siliciclastic laminae in the Wollogorang Formation (DD91HC1–299.8 m). The contact between the middle (coarse) and left (muddy) laminae is interpreted as erosive. Qtz = quartz, K Fel = K-feldspar, Ca = calcite, Py1 = primary (early) pyrite. Way up is indicated above scale bar. 

analyses. Duplicate samples were used to calculate the half absolute relative difference (HARD) for each element analysed (Stanley and Lawie, 2007):

$$\mathrm{HARD} = \left(\frac{\mathrm{assay1}-\mathrm{assay2}}{\mathrm{assay1}-\mathrm{assay2}}\right) * 100$$

Errors of less than 10% were considered acceptable whereas errors greater than 10% were subject to further investigation. Table 1 in the Supplementary information shows the detection limits, analytical method used, and HARD factor for each element analysed. Only Tm and Re returned HARD factors greater than 20% and were earmarked for culling. However, Re is of potential importance to the study so the data were investigated further. Of the 2 samples which were had duplicate multi-element analyses 9 (HC1-03 and RC18-18; Supplementary Info), both of the original analyses and subsequent duplicate analyses showed low Re values, close to or below the LDL (0.002 ppm). Standards used by ACME were also below detection for Re, thus offered no alternative parameter for QA/QC of this element. Due to the potential use of Re, the data were retained with a note of caution. The error is regarded to be at least 0.003 ppm (60% HARD).

### 2.3. Stable isotopes

Sulfides (macroscopic pyrite and chalcopyrite) were analysed for sulfur isotopic composition at Environmental Isotopes Pty., in North Ryde, NSW.

Sulfide samples (<0.1 mg) were hand-picked then combusted in a tin cup using a modified Roboprep elemental analyser attached to a Finnigan 252 mass spectrometer. Samples were analysed relative to an internal gas standard and laboratory standards ($Ag_2S_3$ − +0.4‰ Vienna Cañon Diablo Troilite [VCDT] and CSIRO-S-$SO_4$ + 20.4‰ VCDT). The laboratory standards have been calibrated using international standards IAEA-S1 ($\delta^{34}S = -0.3‰$ VCDT) and NBS-127 ($\delta^{34}S = +20.3‰$ VCDT). Replicate analyses of sulfide standards are within ±0.2‰.

Results are expressed as ‰ $\delta^{34}S$:

$$\delta^{34}S(‰) = \left(\left({}^{34}S/{}^{34}S_{\mathrm{Sample}}\right)/\left({}^{34}S/{}^{32}S_{\mathrm{Standard}}-1\right)\right) \times 1000$$

Where the standard used was the Cañon Diablo Troilite.

### 2.4. Petrography

Multi-method petrographic and semi-quantitative analyses of selected samples were performed at the CSIRO Advanced Characterisation Facility in Perth, WA.

#### 2.4.1. Optical petrography

Transmitted light (TL) and reflected light (RL) petrography was performed using a Zeiss AxioImager system, operated by a Windows PC. Composite high-resolution tiled images of polished thin sections were acquired with a resolution of 2.5 μm on a semi-automated stage.

#### 2.4.2. XRF Mapping

X-Ray Fluorescence (XRF) elemental mapping was performed using a Bruker Tornado M4 XRF Mapper, operated by a Bruker system on a Windows PC. Beam diameter and point spacing of 25 μm was routinely for optimal map resolution, with dwell times varying from 3 to 10 ms depending on sample size.

#### 2.4.3. Field-emission Gun Scanning Electron microscopy (FEG-SEM)

High-resolution element mapping and quantitative mineral geochemistry analyses were performed using a Zeiss UltraPlus Field-emission Gun SEM (FEG-SEM), operated by a Bruker EDX System on a Windows PC.

X-ray mapping was performed using an acceleration voltage of 20 keV and optimal stage working distances of 3–5 mm. Detailed petrography used a range of acceleration voltages and working distances for optimal imagery and X-ray mapping resolution.

## 3. Results

### 3.1. Geochemistry

Concentrations of Zn in all three drill holes range from <20 ppm to >1000 ppm. High grade samples from DD91RC18 and GSD7 have Zn concentrations above detection limit by ICP-MS (10,000 ppm) and were analysed by portable XRF to determine maximum concentrations of 3.04% and 1.55% in GSD7 and DD91RC18, respectively. Lead concentrations range from <10 ppm to ~60 ppm in all three drill holes, with anomalously high values up to 1153 ppm in DD91RC18. Silver concentrations are lowest in GSD7 with a minimum concentration of 32 ppb, and the highest concentrations occur in DD91RC18 where they reach a maximum of 2289 ppb. Fig. 9 shows probability plots of concentrations of Zn, Pb and Ag across the three drill holes.

Transition from a shallow marine to dominantly evaporitic depositional environments in both the McDermott and Wollogorang formations are reflected by clear changes in abundances of trace

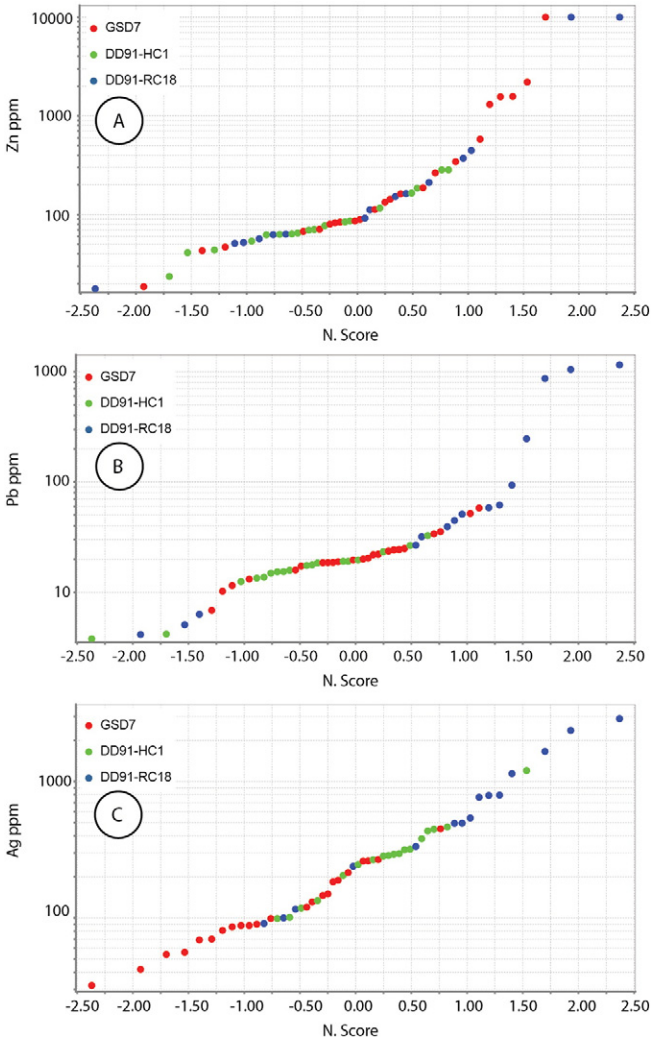


**Fig. 9.** Probability plots of concentrations of A: Zn, B: Pb, C: Ag in the three drill holes analysed, showing distribution and anomalous values. 

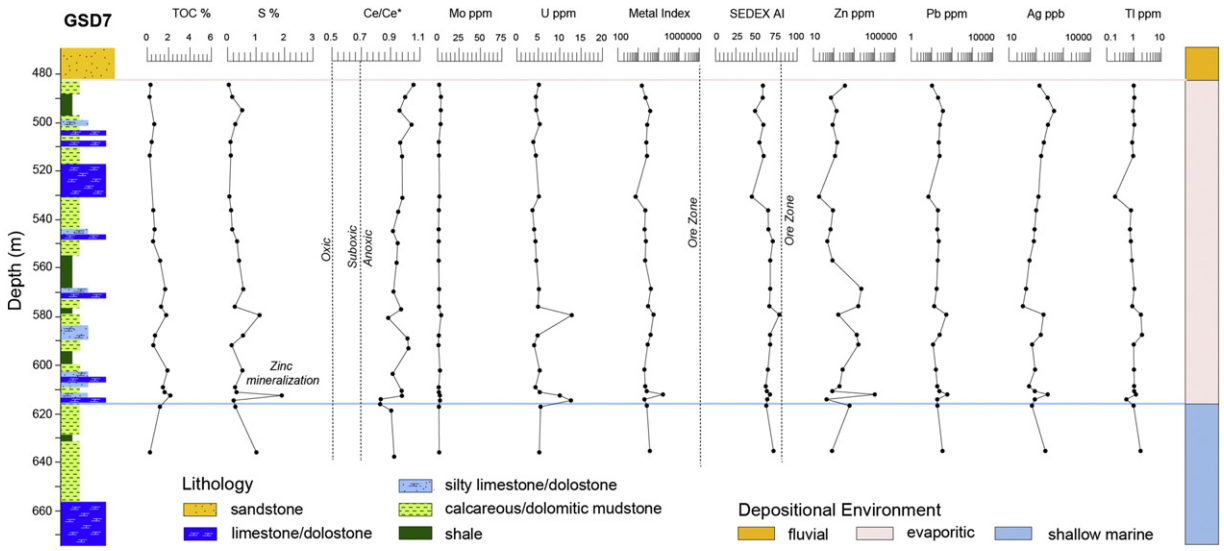


**Fig. 10.** Left: Stratigraphic log of measured section of drillhole GSD7. (Figs. 2, 3) compiled from sedimentological observations and Hylogger spectral mineralogy data. Middle: Downhole geochemical paleoredox and SEDEX metal plots. Right: Interpreted depositional environment. 

elements. The full dataset is available in the Supplementary information. In GSD7 this transition is accompanied by sharp and significant increases in redox-sensitive trace elements such as U and Ce. There are also gradual increases in Zn, Pb, and Ag concentrations which reach a maximum of 3.04% (XRF), 57.92 ppm and 262 ppb, respectively, at 611.9 m depth (Figs. 9, 10). The increases in base metal concertation are closely mirrored by increases in S and TOC concentration, which are as high as 1.88% and 2.1%, respectively, at 611.9 m depth.

In DD91-RC18 the lithological contact is sharp at ~277 m depth, but trace element concentrations are gradational across the transition zone (Figs. 9, 11). Zinc, concentrations increase across the transition to 446.5 ppm at 274.66 m depth, but Pb and Ag concentrations decrease at these depths. Concentrations of Zn reach as high as 1.13 and 1.55% (XRF) at 267.43 and 267.53 m depth, respectively. These depths also have high concentrations of S (2.33%), Pb (1046 ppm) and Ag (2289 ppb). In the overlying carbonaceous unit Zn concentrations decrease but there is an increase in Ag (1662 ppb) and Tl (6.59 ppm) which closely follow large increases in S concentrations which reach 3.48% at 259.6 m depth. These increases are consistent with 'halo' concentrations identified in the favourable unit up to 15 km away from HYC (Large and McGoldrick 2000).

IN DD91-HC1 base metal concentrations are much lower than the stratigraphy of DD91-RC18 (Fig. 9**)**. Zinc concentrations reach 284 ppm at 314 m depth. Concentrations of Pb, Ag and Tl do not markedly increase at this depth but appear to increase in the overlying stratigraphy in a 'halo'-like distribution with maximums of 19.66 ppm, 434 ppb and 4.71 ppm, respectively. A second minor increase in Zn concentrations occurs at 223 m depth (185 ppm), which is mirrored by increases in Pb (32.58 ppm), Ag (1203 ppb) and Tl (8.39 ppm).

### *3.2. Petrographic evidence for base metal sulfide mineralization*

Drill hole DD91RC18 (Wollogorang Fm.) contains abundant stratiform and breccia/fracture-hosted sphalerite mineralization with lesser galena and chalcopyrite. The observed occurrences of stratiform sphalerite occur predominantly in ferroan dolomite laminae, or within

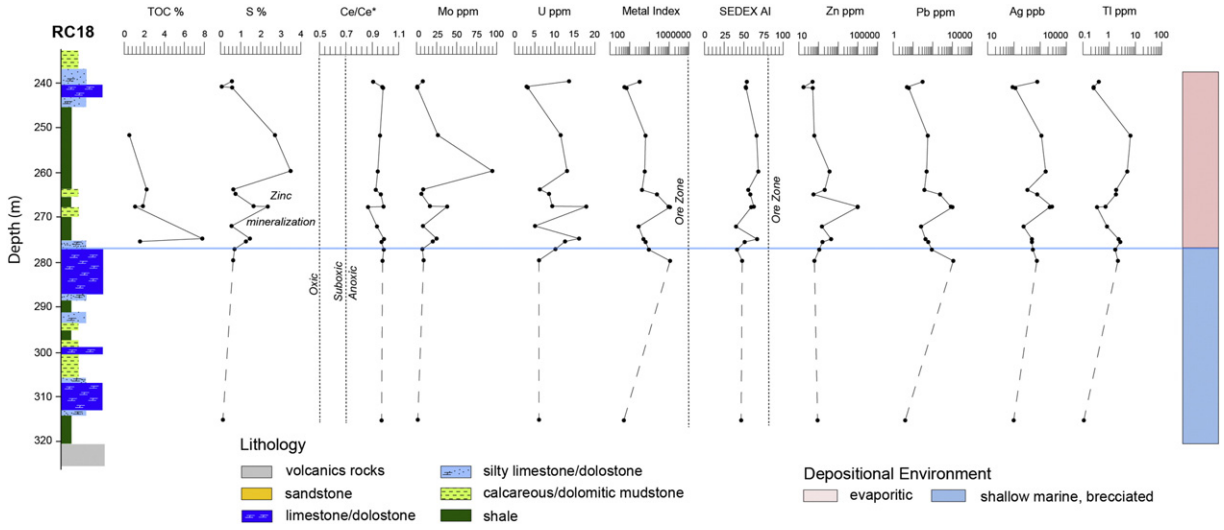


**Fig. 11.** Left: Stratigraphic log of measured section of drillhole DD91RC18. (Figs. 2, 3) compiled from sedimentological observations and Hylogger spectral mineralogy data. Middle: Downhole geochemical paleoredox and SEDEX metal plots. Right: Interpreted depositional environment. 

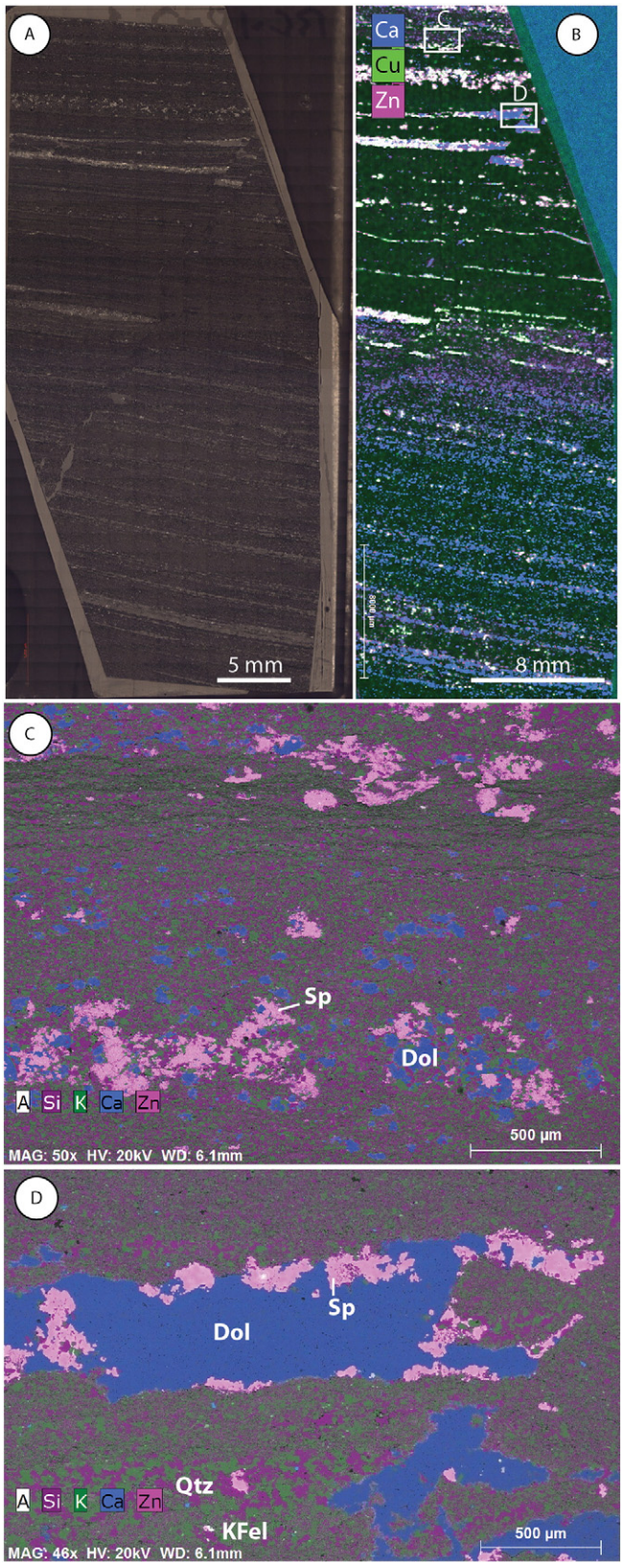


**Fig. 12.** A) Reflected light photomicrograph of section of laminated shale from DD91RC18 267.5 m showing minor fractures and stratiform sulfide mineralization. B) XRF map of field of view in A, highlighting carbonate-associated sphalerite and minor chalcopyrite. Detailed element maps in C and D are highlighted by white boxes. C) FEG-SEM element map highlighting the occurrence of primary (depositional) sphalerite associated with disseminated carbonate. D) FEG-SEM element map highlighting the occurrence of replacement sphalerite within carbonate laminae. 

laminated dolomitic carbonaceous black shale facies (Fig. 12). Base metal sulfides associated with ferroan dolomite laminae commonly display replacement textures on the outer margins where in contact with carbonaceous pyritic facies (Figs. 12, 13). Such replacement textures are locally associated with late pyrite overprinting, suggesting a two-stage mineralization process. Stratiform sphalerite with minor chalcopyrite and galena, perhaps of primary sedimentary origin, occurs as discontinuous crystal aggregates up to 15 mm in diameter associated with both crystalline ferroan dolomite and carbonaceous laminae (Fig. 12). Organic-rich laminae associated with base metal sulfide mineralization in DD91RC18 and DD91HC1 are generally pyritic with fine stratiform bands of early pyrite (Fig. 13). Minor fractures occur within the mineralized laminated black shales, and also commonly contain sphalerite and minor chalcopyrite and galena (Fig. 13).

Breccia-hosted base metal mineralization in drill hole DD91RC18 is characterized by predominantly chalcopyrite > sphalerite which has precipitated around earlier pyrite within angular clasts of black shale, hosted in organic-rich muddy matrix (Fig. 14). Such facies also commonly contain hydrocarbon flows with fine pyrite aggregate flow-fronts.

Similar to drill hole DD91RC18, the sediments of drill hole GSD7 (McDermott Fm.) contain stratiform sphalerite associated with dolomite and ferroan-dolomite laminae in carbonaceous mudstones, again presumably after authigenic carbonate. Base metal sulfides are, however, less abundant in the sediments of GSD7 than DD91RC18. This is coincident with an absence of brecciated shale facies, and less abundant early authigenic/diagenetic pyrite in the shale facies of GSD7. Some minor fractures contain pyrite veinlets that cross-cut sulfide-poor laminated facies.

### 3.3. SEDEX indices

The presence of base metal sulfides in the analysed sections of the Tawallah Group raises the question of ore deposit prospectivity in these sediments. The mineralization style within the alteration halo of HYC (Large and McGoldrick, 2000) is similar to that observed in the McDermott and Wollogorang formations. Sphalerite and other associated base metal sulfides occurs both as fine-grained stratiform layers and in interbedded breccia at HYC (Large et al., 1998). Furthermore, the alteration halo at HYC is characterized by dolomite/ankerite alteration, which has been detected within the target stratigraphic level up to 23 km laterally from the main orebody (Large et al., 2000). The SEDEX mineralization indices (Large and McGoldrick, 2000; Large et al., 2000) have been applied here to the McDermott and Wollogorang formations to test for SEDEX signals.

#### 3.3.1. SEDEX metal index

The SEDEX Metal Index (MI) is a method of combining target and pathfinder elements of SEDEX deposits, taking into account the limited lateral dispersion of Pb, and widespread dispersion of Tl (Large et al., 2000; Large and McGoldrick, 2000):

$$SEDEX\,Metal\,Index = Zn + 100Pb + 100Tl$$

Assessments of drill cores from HYC deposit yield SEDEX MI factors greater than $10^6$ within the ore zone, and up to just over $10^5$ in the same stratigraphic level 15 km away (Large et al., 2000).

The highest SEDEX MI in GSD7 was over $10^4$ with a factor of 15,910 at 612 m depth. This is attributed to high concentrations of Pb (58 ppm) and Zn (30,400 ppm; SI Table 2; Figs. 9, 10). The SEDEX MI factor in DD91RC18 reaches higher than $10^5$, with factors of over 114,000 at 267.43 m depth (868 ppm Pb, 11,300 ppm Zn) and over 115,000 at 279.5 m depth (1154 ppm Pb, 63 ppm Zn; SI Table 2; Figs. 9, 11). The latter is the highest SEDEX MI factor observed in this study, though it is noted that the Zn concentrations at this depth are low.

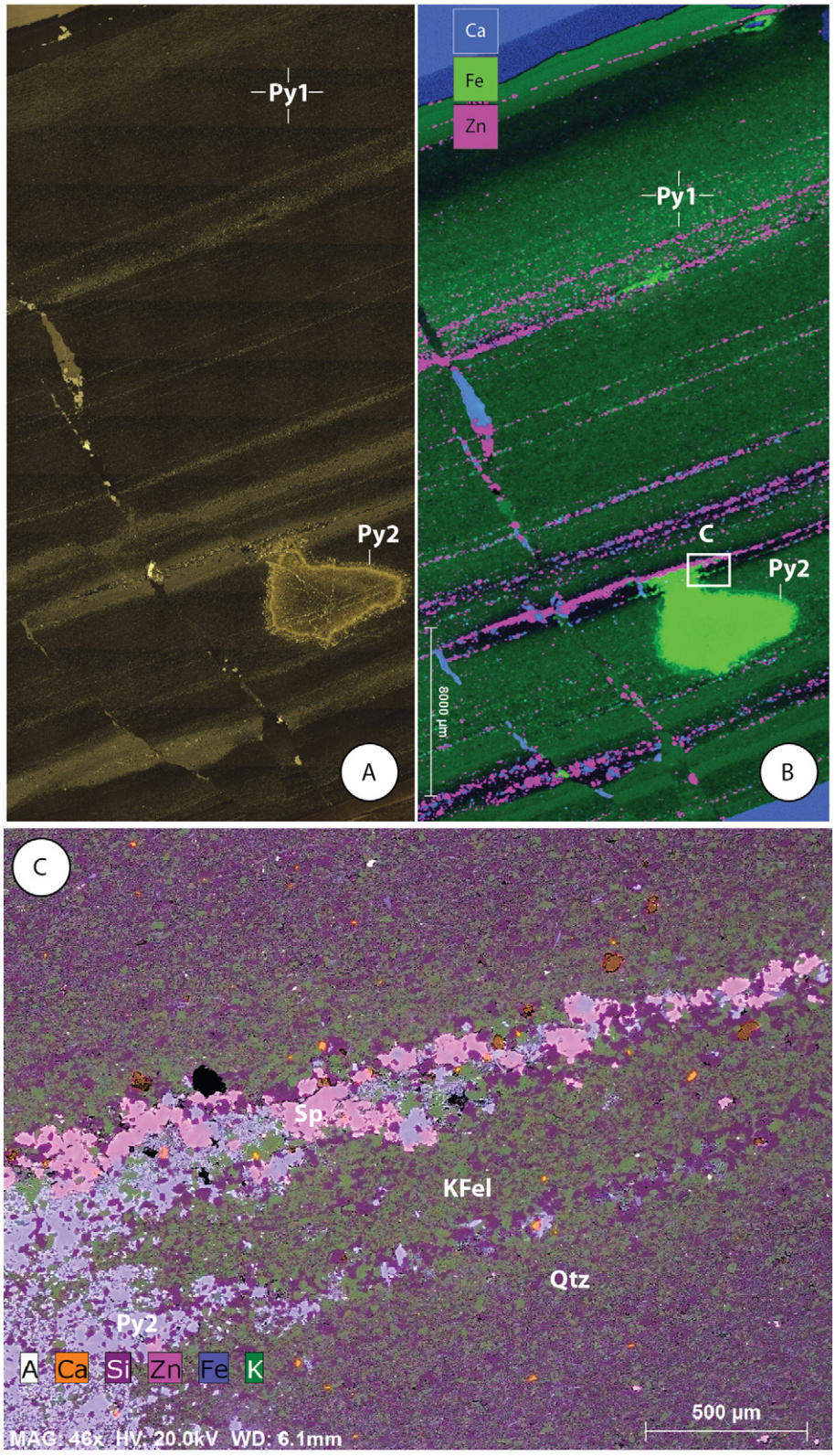


**Fig. 13.** A) Reflected light micrograph of laminated shale from DD91RC18 267.4 highlighting laminated and minor vein sphalerite, primary (early) pyrite (Py1) and late-stage overprinting pyrite nodule (Py2). B) XRF map of field of view in A, highlighting laminated sphalerite and overprinting Py2 pyrite. Sp = sphalerite, Py1 = pyrite 1, Py2 = pyrite 2. C) FEG-SEM element map highlighting the occurrence of laminated sphalerite within silty laminae and overprinting by Py2. Qtz = Quartz, K Fel = K feldspar, Sp = Sphalerite, Py = Pyrite. 

The roughly equivalent stratigraphic level within the Wollogorang Fm. Drill hole DD91HC1 has a SEDEX MI factor of just over $10^2$ at ~2325–2465 between 293 and 314 m depth, even though Zn and Pb are not particularly enriched at this depth in DD91HC1. The highest MI in HC1 Is 4168 at 223.85 depth, where there is no elevation in Zn or Pb but a slightly enriched Tl value of 8.39 ppm (SI Table 2).

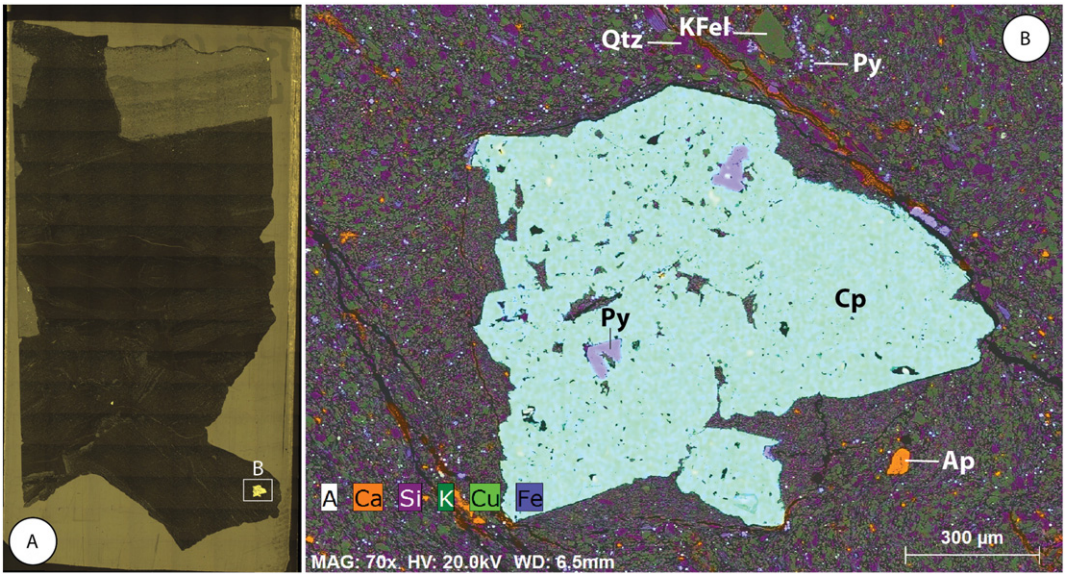


**Fig. 14.** A) Reflected light micrograph of brecciated Wollogorang Formation from DD91RC18 275.3 m which contains clasts of locally-sulfidic black carbonaceous siltstone and light evaporitic facies. B) FEG-SEM element map of chalcopyrite mass within a fine muddy breccia clast surrounded by a silt flow. The crystal mass appears to have mineralized around primary pyrite. Qtz = Quartz, K Fel = K feldspar, Cp = Chalcopyrite, Py = Pyrite, Ap = Apatite. 

### 3.3.2. SEDEX alteration index

The SEDEX Alteration Index (AI) is a means of mapping alteration haloes around SEDEX deposits, and is controlled by three primary factors: i) increased content of Mn and Fe in carbonate during replacement of MgO, ii) increase in pyrite (FeO) in carbonaceous facies, and iii) increased shale/dolomite ratio (MgO). Large et al., (2000) demonstrated that these three factors all increase with proximity to Australian Proterozoic SEDEX deposits. There are lithological factors which affect the SEDEX AI such as lateral changes between dolomite and shale, which would affect the ratio of MgO and $SiO_2/Al_2O_3$ and thus the SEDEX AI score. Different SEDEX AIs are used to account for lithological criteria (Large et al., 2000; Large and McGoldrick, 2000):

$$\text{SEDEX AI} = (\text{FeO} + 10\text{MnO}) * 100/(\text{FeO} + 10\text{MnO} + \text{MgO})$$

$$\text{SEDEX AI 3} = (\text{FeO} + 10\text{MnO}) * 100/(\text{FeO} + 10\text{MnO} + \text{Al}_2\text{O}_3)$$

$$\text{SEDEX AI 4} = (\text{FeO} + 10\text{MnO}) * 100/(\text{FeO} + 10\text{MnO} + (\text{SiO}_2/10))$$

Replacing the denominator of MgO in the AI with $Al_2O_3$ (SEDEX AI 3) and $SiO_2$ (SEDEX AI 4) in all cases reduces the AI score. In the absence of any known proximal SEDEX deposit, it is impossible to base any one of the SEDEX AI models as a proximity vector to mineralization. Rather, the standard SEDEX AI is used here as an indicator of base metal potential over barren background sediments.

SEDEX AI values of 80 to 100 are observed within ore-zone mineralized sediments, whereas background barren sediments have values of 0 to 40 (Fig. 15; Large et al., 2000; Large and McGoldrick, 2000). Increasing SEDEX AI values with concomitant increases in Zn are indicative of increasing proximity to SEDEX-type mineralization.

Many of the samples from GSD7 plot close to the ore field (Fig. 15), and none plot within the barren lithology field, reflecting enrichment in Zn, Pb and Tl. In DD91RC18, the maximum SEDEX AI value is ~69. Indeed, this section of stratigraphy in RC18 (~260–280 m depth) yielded high Zn, Pb and Cu values in both this study (Fig. 11) and in the original exploration assays. HC1 has moderate SEDEX AI values with up to 283 ppm Zn. While these values are elevated above the background barren lithologies, they are consistently lower than the values for RC18 (Fig. 9).

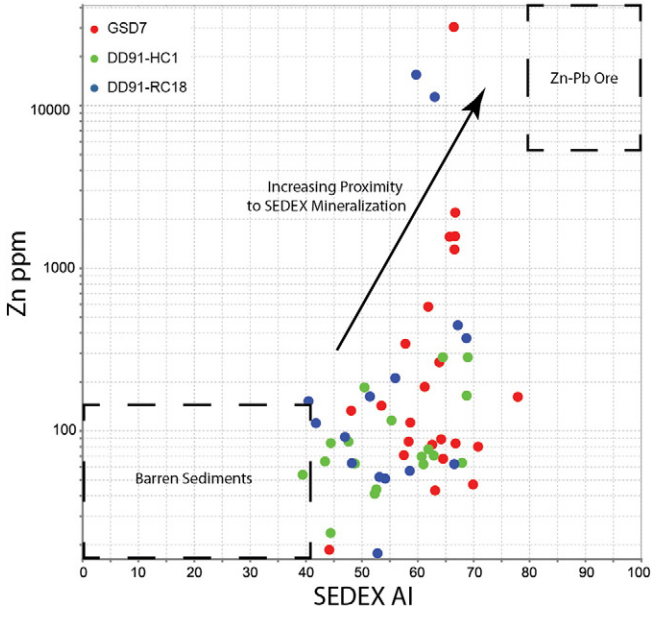


**Fig. 15.** SEDEX Alteration Index versus Zn plot of DD91RC18, DD91HC1 and GSD7 including additional pXRF analysis for ADL Zn samples. Figure modified from Large et al. (2000); Large and McGoldrick, 2000). 

### 3.4. Paleoenvironment

Determining the paleoredox conditions of shales using whole-rock multi-element analysis is complex. There are no unilateral analytical methods available which can be used to accurately measure the paleoredox environment of all shales. Those which are used have significant geochemical and statistical complications (see Xu et al., 2012 for review). A common method for interpreting the paleoredox conditions in shales is to assess of ratios of redox-sensitive elements within the

rock, such iron species ratios or degree of pyritisation. Many factors that can affect the contribution of each element to sedimentary rocks must be taken into account when using elemental ratios to interpret paleoredox conditions. These factors include the composition of detrital clastic sedimentary material, any dissolved aqueous authigenic contribution to the sediment, and potential diagenetic or metamorphic remobilization of some elements. Near-shore shallow marine environments, such as those in which the shales of DD91HC1, DD91RC18 and GSD7 can be subject to relatively high detrital sediment fluxes, such that the facies can have concentrations of authigenic trace metals diluted by detrital grains. As such, well-known and regularly used paleoredox proxies of redox-sensitive elements plotted against Ni/Co, V/(V + Ni), V/Cr and U/Th from the whole-rock analysis in this study resulted in contradictory interpretations (i.e. both oxic and anoxic) based on previous paleoredox studies (e.g. Xu et al., 2012 and references therein). These possible interpretations are largely based on the concentration of detritally-derived element ratio pairs residing in similar sediment phases such as Ni and Co adsorption in sedimentary sulfides, and Cr-bearing clay minerals. Both clay minerals and sedimentary sulfides are present, though not ubiquitously, in the samples analysed in this study. Given the significant detrital input to the sediment these proxies are not considered further here. Paleoredox proxies using elements of predominantly dissolved aquatic or authigenic source, such as soluble REEs, Re, Mo, S and TOC were instead used.

### 3.4.1. Trace element proxies

*3.4.1.1. Ce/Ce*.* Of the rare earth elements (REEs), only cerium (Ce) and europium (Eu) are redox-sensitive (German and Elderfield, 1990; Cullers, 2002; Slack et al., 2007). Cerium concentrations in shales relative to other REEs can be used to interpret the paleoredox conditions of the sediment–water interface during deposition as Ce oxidizes from 3 + to insoluble 4 + state in oxidising water whereas the other REEs remain soluble. Cerium 4 + is deposited and enriched in the sediment relative to other REEs under oxidizing conditions, and is not enriched under anoxic conditions (German and Elderfield, 1990). This redox-sensitive behaviour of Ce is incorporated into the Ce/Ce* index:

$$Ce/Ce* = 3 * (Ce_{Sample}/Ce_{Average})/((2 * La_{Sample}/La_{Average}) + (Nd_{Sample}/Nd_{Average}))$$

Where Sample is the REE element analysed in this study, and Average is the REE element concentration in an average shale. In this case the Post-Archean Australian Shale (Nance and Taylor, 1976) was used.

Ce/Ce* values of ~0.06–0.5 occur in well oxidized modern seawater and 0.6–0.7 in suboxic modern seawater (Cullers, 2002; Slack et al., 2007) due to the oxidative removal of Ce, whereas more positive values close to 1.0 or more occur in anoxic sediments enriched in Ce (Cullers, 2002). However, this index assumes Ce, La and Nd concentrations in the sediment during deposition have not been altered during diagenesis or any subsequent alteration events. Modern hydrothermal sediments have been known to exhibit negative Ce anomalies (German and Elderfield, 1990) similar to oxidised seawater, thus the redox potential of hydrothermal or SEDEX fluids must be taken into account for Ce/Ce* values in Proterozoic McArthur Basin shales.

Observed Ce/Ce* values are consistently between approximately 0.9–1.1 throughout DD91RC18, DD91HC1 and GSD7 (Figs. 10, 11). This is consistent with deposition under strongly anoxic conditions (Cullers, 2002; Slack et al., 2007). There are Ce/Ce* anomalies as negative as 0.87 and 0.83 in DD91RC18 and GSD7 respectively. These low values are markedly less positive than the rest of the samples analysed in each drill hole, and perhaps importantly, they coincide with Zn mineralization. This may reflect oxidative hydrothermal or SEDEX fluid-induced enrichment of Ce relative to other REEs in the sediment, as these samples have the highest Ce values in DD91RC18 and GSD7 at 255 and 92 ppm respectively (Supplementary information Table 2).

*3.4.1.2. Re v Mo.* Ratios of rhenium (Re) and molybdenum (Mo) in shales are useful in distinguishing anoxic sulfur-poor and euxinic depositional conditions due to their distinctive behaviour across different sulfur-redox boundaries. Both Re and Mo have a low detrital component, thus their accumulation in sediments largely represent authigenic input from dissolved aqueous source. Rhenium is insoluble in anoxic conditions and is thus enriched in sediments deposited in reducing environments (Crusius et al., 1996). Molybdenum has a strong affinity for sulfidic environments. It is sequestered by organic matter and sulfide during and/or soon after deposition at the sediment–water interface in euxinic conditions. Molybdenum is not enriched in non-sulfidic anoxic environments (Crusius et al., 1996). High Re/Mo ratios in sediments reflect deposition under anoxic, sulfide-poor conditions, as Re is enriched relative to Mo. Low Re/Mo ratios reflect deposition under euxinic conditions (Crusius et al., 1996; Ross and Bustin, 2009).

All samples analysed had low concentrations of Re, some of which were below detection limit. Both DD91RC18 and DD91HC1 samples plot across the euxinic-anoxic boundary due to their comparatively high Mo concentrations, which suggests deposition under anoxic and intermittent euxinic conditions (Fig. 16). The sediments of GSD7 have very low Re and Mo concentrations, and plot mostly within the anoxic field. These interpretations assume that Re was not remobilised during hydrothermal alteration, and that the delivery of Mo to the sediments during deposition was authigenic sequestration onto organic matter and sulfide, and not later sulfide mineralization events.

*3.4.1.3. V/Mo v Mo.* Under reducing conditions, vanadium can be enriched in sediments mainly through adsorption onto clays and organic matter (Xu et al., 2012) Molybdenum is only enriched in sediment under euxinic conditions (Crusius et al., 1996). High V/Mo ratios in sediments therefore suggest deposition under anoxic, sulfur-deficient conditions, whereas low V/Mo ratios (i.e. high Mo) in sediment are more indicative of Mo enrichment by deposition under euxinic conditions (Piper and Calvert, 2009).

When applied to the analyses in this study, the V/Mo ratios suggest that sedimentary rocks in DD91RC18 and DD91HC1 were deposited under mostly euxinic conditions, however the ratios for sedimentary rocks in GSD7 suggest they were deposited under mostly anoxic conditions (Fig. 16).

*3.4.1.4. TOC v S.* Ratios of TOC and S can be useful for determining aquatic environments based on sulfur input during deposition, or for identifying post-depositional sulfur input in post-Archean shales (Leventhal, 1995). Low S concentrations in shales with varying TOC contents are indicative of deposition within sulfur-limited basins (Berner and Raiswell, 1984). Positive correlations of TOC and S represent deposition in normal open marine environments where sulfate-reducing bacteria provide the $H_2S$ needed for pyrite incorporation to the sediment (Berner, 1983; Berner and Rasiwell, 1983; 1984; Leventhal, 1995; Canfield, 2004). High sulfur concentrations with varying TOC contents represent euxinic conditions with sulfide precipitation in the water column providing excess sulfur to the sediment. Very low TOC–S ratios with high S and low TOC can represent post-depositional addition of sulfur to sediment, such as an influx of sulfur-rich mineralizing fluid causing sulfide precipitation (Leventhal, 1995).

In this study, the TOC–S ratios show unclear relationships for each drill hole, with no clear trend. This is interpreted to be a result of intermittent euxinia and anoxia during deposition, and also localized sulfur overprint during post-depositional sulfide mineralization (Fig. 16).

The Wollogorang Formation rocks have TOC–S ratios consistent with deposition under intermittent euxinia and anoxic environments (Fig. 16). Samples from DD91RC18 show evidence for significant overprinting of S, with some sediments hosting stratiform base metal sulfide mineralization. Interestingly, Zn mineralization is associated with TOC–S ratios

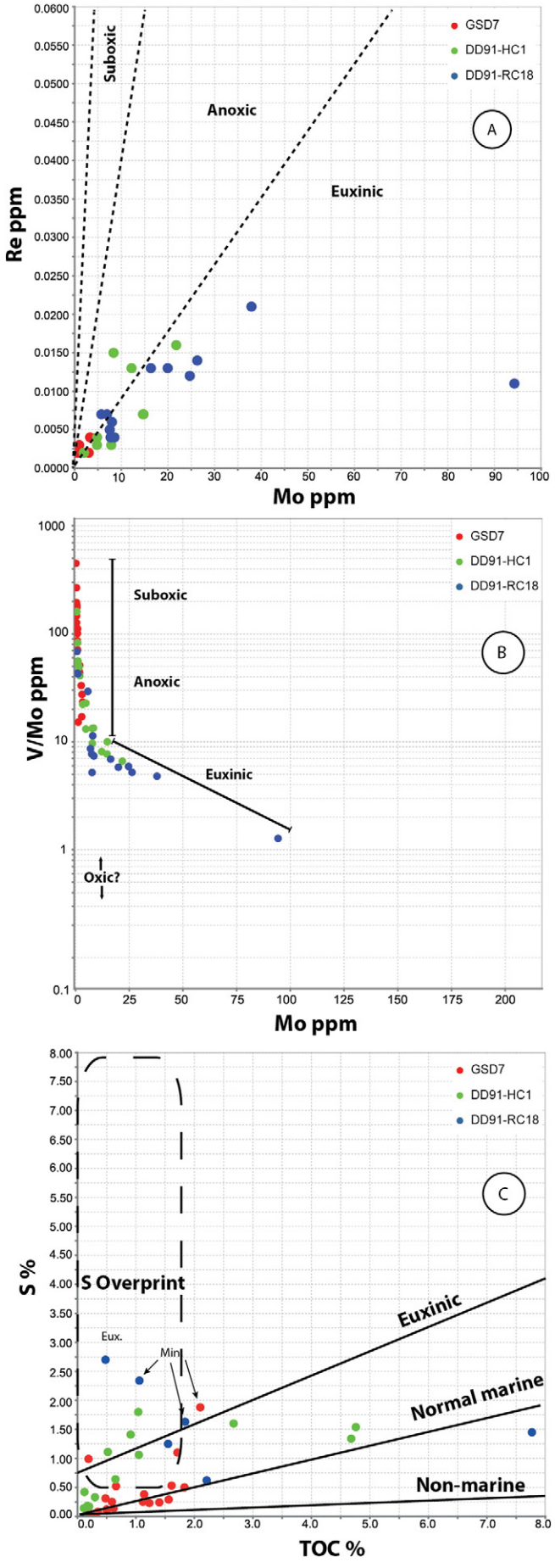


which show a strong euxinic signal. Non-mineralized sediments which show a weak euxinic signal from TOC–S ratios, suggesting a genetic relationship between mineralization and authigenic sulfides (euxinia) within the sediment.

Abundant stratiform pyrite in non-mineralized carbonaceous facies within drill holes DD91RC18 and DD91HC1 (Fig. 8) provide further petrographic evidence for euxinic depositional conditions. These finely disseminated and laminated pyrite layers are interpreted to represent either syndepositional or early diagenetic precipitation of pyrite from $H_2S$-rich bottom waters or pore-water in the shallow sediment, and are consistent with the occurrence of early pyrite at HYC (e.g. Ireland et al., 2004).

The TOC-S ratios of sedimentary rocks of the McDermott Formation in GSD7 suggest deposition predominantly in a sulfur-limited environment, with few intermittent sulfidic events. This may reflect poor access to the open marine environment such as an epeiric intracratonic basin or lake, or globally-low oceanic sulfate at that time (e.g. Shen et al., 2002). Similar to the Wollogorang Formation rocks intersected in DD91RC18, the rocks in GSD7 were also subject to replacement-style Zn mineralization.

### 3.4.2. Sulfur isotopes

The S isotope compositions of stratiform and fracture-hosted pyrite in DD91HC1 and DD91RC18 range between +14.5 and −11.7‰ with a mean of 1.5‰ (Table 1), similar to stratiform sulfides in other shale deposits of similar age (Fig. 17). A $\delta^{34}S$ value of 0.7 ‰ from stratiform sulfide within DD91HC1 is consistent with bacterial sulfate reduction of seawater sulfate that had $\delta^{34}S$ values of ~15–25‰ during that time (Strauss, 1993), in a sulfur-limited shallow marine shelf environment where sulfate becomes depleted due to active bacterial sulfate reduction (Shen et al., 2002).

Some of the base metal sulfides in DD91RC18 apparently formed as a result of interaction between metalliferous sulfate-bearing brines with sedimentary pyrite, because they are associated minor trace sulfate inclusions. As a result of the analytical method used, these heterogeneous sulfate-bearing sulfide phases are likely to have yielded composite $\delta^{34}S$ values that are enriched in $^{34}S$ relative to a pure sulfide sample. Thus it is possible that $\delta^{34}S$ values for some sulfides analysed in DD91RC18 are elevated due to the localized presence of sulfate inclusions.

The sulfidic shale facies of the McDermott Formation in GSD7 did not yield macroscopic sulfide grains, as all identified sulfide is finely disseminated with grains and clusters typically <5 μm. As such no S isotope data could be acquired for the McDermott Formation as part of this study with the method used.

## 4. Discussion

### 4.1. Paleoenvironmental implications for SEDEX-Style Base metal deposition at 1.7 Ga

#### 4.1.1. REEs

While the mechanisms of McArthur-type SEDEX base metal deposition are complex, it is generally understood that redox conditions of the bottom waters and pore fluids is a first-order control

**Fig. 16.** Paleoredox plots. A) Re versus Mo paleo-redox plot. Re is generally highly-enriched in anoxic sediments and to a lesser extent in euxinic sediments, whereas Mo is highly-enriched in euxinic sediments. Figure modified from Crusius et al. (1996) and Ross and Bustin (2009). B) V/Mo versus Mo paleo-redox plot for all analysed samples from DD91RC18, DD91HC1 and GSD7. Low V/Mo ratios and high Mo concentrations indicate euxinic depositional environments, whereas high V/Mo ratios and low Mo concentrations indicate suboxic-anoxic depositional environments. Plot modified from Piper and Calvert (2009) and Xu et al. (2012). C) TOC versus S plot for all analysed samples from DD91RC18, DD91HC1 and GSD7. Idealized plot areas for non-marine, normal marine and euxinic depositional environments are shown. Some GSD7 samples plot within the non-marine zone. Samples which plot in the S overprint zone are either euxinic (Eux.) or have been subject to mineralization (Min.) or a combination of both. Plot modified from Leventhal (1995). 

**Table 1**
Sulfur isotope data from Wollogorang Formation.

| Hole ID | Sample ID | Depth (m) | $\delta^{34}S$ raw | $\delta^{34}S$ ‰ VCDT | Sulfide type |
|---|---|---|---|---|---|
| GSD-7 | sGSD7-29 | 611.9 | ts | N/A | Stratiform |
| DD91HC1 | sHC1-16 | 223.95 | ts | N/A | Stratiform |
| DD91HC1 | sHC1-17 | 256.05 | 4.0 | 0.7 | Stratiform |
| DD91HC1 | sHC1-22 | 339.2 | ts | N/A | Stratiform |
| DD91RC18 | sRC18-2.1 | 267.53 | 5.6 | 1.6 | Fracture fill and disseminated sulfide |
| DD91RC18 | sRC18-2.2 | 267.53 | 6.3 | 2.3 | Fracture fill |
| DD91RC18 | sRC18-3 | 274.66 | 8.2 | 5.0 | Slump |
| DD91RC18 | sRC18-4 | 275.3 | 8.4 | 4.6 | Slump |
| DD91RC18 | sRC18-9 | 239.6 | 3.5 | −0.6 | Slump |
| DD91RC18 | sRC18-10 | 240.8 | 9.3 | 5.4 | Fracture fill |
| DD91RC18 | sRC18-11 | 241 | −6.9 | −11.7 | Fracture fill |
| DD91RC18 | sRC18-14 | 264.7 | 17.4 | 14.5 | Fracture fill |
| DD91RC18 | sRC18-15 | 267.43 | −2.4 | −6.4 | Fracture fill |
| DD91RC18 | sRC18-16 | 271.85 | ts | N/A | Fracture fill |
| DD91RC18 | sRC18-17 | 277 | ts | N/A | Fracture fill |
| DD91RC18 | sRC18-18 | 279.5 | ts | N/A | Fracture fill |

Table 1. Sulfur isotope data.


on mineralizing metallic brines (Cooke et al., 2000). Such deposits contain large amounts of sedimentary sulfur, which is likely sourced independently from $H_2S$ in euxinic bottom waters as a result of bacterial reduction of seawater sulfate (Lyons et al., 2006). Thus oceanic euxinia, at least on a local scale, is required for the formation of McArthur-type SEDEX deposits.

The emergence of oceanic euxinia is thought to have occurred ~1.8 Ga, which coincides with the disappearance of banded iron formations (BIFs) and, strikingly, the arrival of sedimentary SEDEX deposits in black shales (Lyons et al., 2006). Previous assertions that the cessation of BIF deposition reflected deep oceanic oxygenation (Holland, 2005), or widespread euxinic conditions (Canfield, 1998), have been disputed with evidence for co-existence of ferruginous and euxinic conditions in the oceans from the Neoarchean to the Neoproterozoic (Planavsky et al., 2011). There is an emerging model of euxinia occurring along continental margins (Poulton et al., 2010) and localised intracontinental sub-basins, while the deep oceans may have remained ferruginous (Planavsky et al., 2011). The sediments analysed in this study are interpreted to have been deposited in such marginal marine settings, which raises the possibility of the development of euxinic bottom waters (Poulton et al., 2010).

The results of analyses of redox-sensitive trace element paleoredox proxies suggest that both the McDermott and Wollogorang formations were deposited under fluctuating redox conditions. REE-Cerium dynamics imply almost ubiquitous deposition under extreme anoxic conditions (Figs. 10, 11,). A curious enrichment of Ce and subsequent slightly negative Ce/Ce* anomaly in sediments associated with Zn sulfide mineralization (Figs. 10, 11) may represent an input of oxidised metallic brine into the shallow reduced sediment, partly oxidising dissolved $Ce^{3+}$ in the shallow pore fluids to insoluble $Ce^{4+}$ (German and Elderfield, 1990).

*4.1.2. Trace Elements*

Molybdenum, V, and Re ratios throughout the McDermott Formation (Fig. 16) are largely consistent with petrographic evidence for the sediments having been mostly deposited under moderately sulfidic anoxic conditions with intermittent high influx of marine sulfate into the basin at the site of deposition of the GSD7 sediments. Euxinic sediments occur close to the bottom of the analysed section of GSD7, between 568 and 612 m depth, but sulfur concentrations decreased as the basin shallowed. The cause of this remains uncertain, it may reflect reducing concentrations of marine sulfate during the deposition in that part of the basin.

Several factors may have affected the flux of sulfate to the McDermott Formation basin. The basal shales of GSD7 are interpreted to have been deposited in a platform-type marginal environment, of which slightly older equivalents in the Animike Basin are thought to have been euxinic (Poulton et al., 2010). Low sulfur concentrations in the evaporitic shale facies higher in the stratigraphy of GSD7 may reflect the development of a sulfur-poor shallow marine environment, however given the shallowing of the basin and progression to fluvially-dominated siliciclastic deposition, the possibility of the basin being closed to the open ocean and therefore to a sulfate source cannot be discounted. The paucity of sulfidic facies in the upper section of the basal McDermott Formation stratigraphy analyzed in this study reduces the prospectivity for mineralization in those rocks, whereas the sulfidic basal shales are considered prospective.

The Wollogorang Formation sediments are rich in laminae of micron-scale euhedral pyrite crystals and clusters in the carbonaceous facies. Such textures are consistent with deposition under euxinic conditions, and trace element and C/S ratios similarly indicate abundant sulfur in the water column or pore fluids. Enhanced Mo concentrations relative to Re and V in analysed sections of carbonaceous shales signals uptake of Mo into authigenic sulfides and organic matter under euxinic

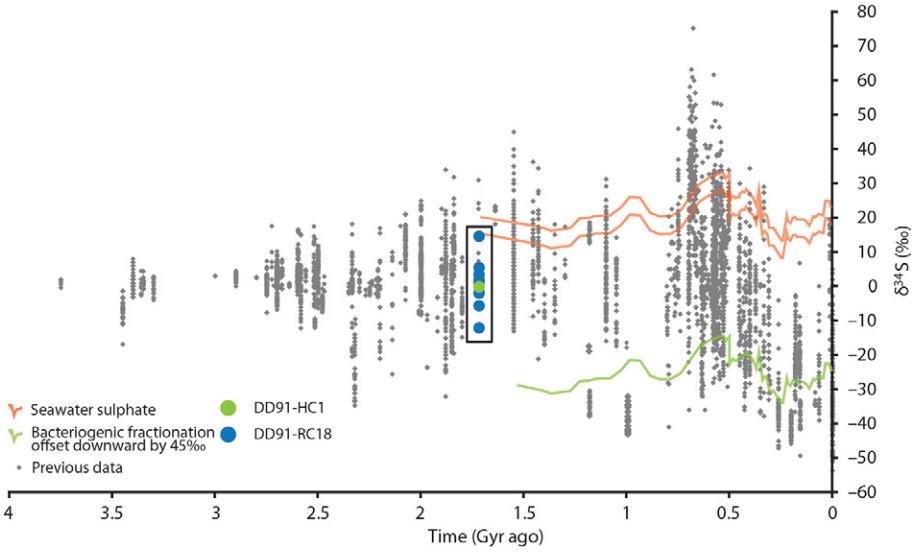


**Fig. 17.** $\delta^{34}S$ isotope compilation from sulfides in marine shales through geological time. Data from this study are consistent with other bacteriogenic early Mesoproterozoic marine sulfides. Figure and data modified from Parnell et al. (2010). 

conditions. The high degree of pyritization (DOP) in other sections of the Wollogorang Formation are comparable to the typical modern euxinic sediments of the Black Sea (c.f. Shen et al., 2002).

While not all of the analyzed sections of the Wollogorang Formation display trace element and petrographic evidence for extremely euxinic conditions, none are sulfur-poor. This may be the result of a restricted marine environment that was not permanently linked to the open-ocean or a localized sulfate source, with episodic influxes of sulfur. The range of $\delta^{34}S$ values from the sedimentary sulfides (+14.5 and −11.7‰; Fig. 17) is comparable with the $\delta^{34}S$ values in other sections of the Wollogorang Formation (Shen et al., 2002) and to early pyrite from the younger HYC deposit (Ireland et al., 2004; Lyons et al., 2006). Sulfate reducing bacteria preferentially use the $^{32}S$ isotope. This results in enrichment of $^{32}S$ and depletion of $^{34}S$ ($\delta^{34}S$ ‰) in biogenic sulfide relative to the parent sulfate by up to ~45‰ in non-sulfate limited basins with access to the open ocean or a sulfur reservoir (e.g. Parnell et al., 2010). Sediments deposited under normal non sulfate-limited modern marine conditions typically have a large range in $\delta^{34}S$ values that reflect homogenous redox conditions during deposition and pore water sulfide evolution during diagenesis (Canfield and Teske, 1996; Shen et al., 2002). Laminated sulfides deposited under ubiquitously euxinic conditions have a much smaller range of low $\delta^{34}S$ ($^{32}S$ enriched) values, as observed in the Black Sea (Shen et al., 2002 and references therein).

In sulfate limited basins such as intracratonic seas or lakes that are not openly linked to the global oceanic sulfate reservoir or a local source, dissolved sulfate can be readily depleted by bacterial sulfate reduction and concomitant deposition of pyrite. As the inventory of $^{32}S$ is depleted, lower degrees of isotopic fractionation from parent sulfate in sedimentary sulfides occur, which results in higher $\delta^{34}S$ ($^{34}S$ enriched) values (Shen et al., 2002). Thus the range of $\delta^{34}S$ values in early sulfides in the analysed sections of the Wollogorang Formation of +14.5 and −11.7‰ may, at least on a localised basin level, reflect heterogenous availability of dissolved sulfate in the water column with periodic depletion in $^{32}S$ by bacterial sulfate reduction. This suggests that the site of deposition was euxinic, but subject to ephemeral sulfate flux. Such euxinic depositional conditions would have been favourable for the deposition and preservation of sulfides and organic matter, improving the oxidized brine-reducing potential of the sediments (Cooke et al., 2000).

### 4.2. Sulfide deposition

The two distinct styles of base metal sulfide mineralization observed in the McDermott and Wollogorang formations are comparable with occurrences distal to the large McArthur type deposits such as HYC (e.g. Large et al., 1998; 2000; 2005; Large and McGoldrick, 2000; Cooke et al., 2000; Ireland et al., 2004). Chalcopyrite, not common at HYC, and sphalerite growth around early pyrite in mudstone clasts (Fig. 14) in sedimentary breccia zones implies the presence of metalliferous fluids during or soon after slumping, which may have been expelled from deeper sediments through fault zones in the measured sections of the McDermott or Wollogorang formations (Large et al., 2005). No laminated depositional sphalerite have been observed comparable to the occurrences close to the major fault structures at HYC (e.g. Large et al., 1998) implying a distal locality for the sulfide occurrence.

The presence of Cu sulfides in the analysed sections of the Wollogorang Formation may have implications for the source of Cu in the Redbank Cu deposits (Rod, 1978; Knutson et al., 1979; Redbank Copper Ltd. 2010; Ahmad et al., 2013). These deposits occur within breccia pipes that transect the Settlement Creek Volcanics, Wollogorang Formation and Gold Creek Volcanics. The breccia pipes are thought to have formed as a result of explosive release of fluids during magmatic emplacement at depth (Knutson et al., 1979), with consequent hydrothermal circulation of connate brines. The brines remobilized metals, mainly Cu, from the sedimentary and volcanic lithologies, leading to precipitation of Cu sulfide within the breccia zone between the Wollogorang Formation and Gold Creek Volcanics (Knutson et al., 1979). The presence of Cu sulfides in the Wollogorang Formation in DD91RC18 is consistent with the model of remobilization of Cu from sediments during explosive brecciation and hydrothermal fluid flow. This is supported by the presence of pyrobitumen in some breccia pipes within the Redbank area (Ahmad et al., 2013), which are likely to have been sourced from the carbonaceous lithologies of the Wollogorang Formation.

Stratiform sphalerite observed in several horizons of laminated shale, particularly evident in the Wollogorang Formation (Fig. 12) occur within bedding-parallel zones of ferroan dolomite or ankerite alteration that have replaced the original sediment, presumably authigenic carbonate, interbedded between pyritic carbonaceous laminae. The original composition of the replaced sediment is not preserved, and is thus unknown, but replacement textures imply fluid flow through a permeable clastic or authigenic carbonate facies. Such sphalerite-bearing laminae are comparable to Stage 2 sphalerite at HYC (Ireland et al., 2004) which were overprinted by late stage pyrite nodular aggregates. Cooke et al. (2000) argued that reduced acidic metal brines would not retain their metal load while being transported through carbonate-bearing stratigraphy due to the pH buffering on base metal solubilities. Conversely, this would not be the case in some scenarios. If pressure and temperature of fluids were high enough, ~50 bar at 250 °C, fluids could still be acidic due to the high concentrations of carbonic acid. Similarly, if fluid flow through carbonate stratigraphy was fast enough, fluids would not have time to equilibrate with the carbonate, thus retaining at least part of their metal load. This scenario is most likely the case at HYC (David Cooke, pers. comm.) Carbonate stratigraphy occurs in the lower parts of both the McDermott and Wollogorang formations. This implies that either the metal-bearing fluids responsible for replacement-style base metal deposition were not reduced and acidic, or that fluid flow through the carbonate stratigraphy was fast enough to prevent buffering. The oxidised hematitic and evaporitic units underlying the lower Tawallah Group (Ahmad et al., 2013) most likely buffered basinal fluids to oxidising and saline brines. It is these Tawallah Group-derived basinal brines which are thought to be the source for the mineralisation at HYC within the overlying McArthur Group (Cooke et al., 2000). Furthermore, the Siegel Volcanics, which lie beneath the McDermott Formation (Fig. 3) are leached of metals and have been K metasomatised (Cooke et al., 1998), presumably by oxidized fluids. The presence of oxidising saline brines within the basin would be efficient at leaching base metals from the volcanics, thus providing a metal source for potential SEDEX style mineralization. Replacement stratiform sphalerite commonly occurs at the boundary between reduced-pyritic carbonaceous and carbonate lithologies, which is consistent with a model of oxidizing brines depositing base metal sulfides upon contact with reducing stratigraphy.

### 4.3. SEDEX indices

At HYC there are pronounced lithogeochemical haloes associated with mineralization which extend several kilometres from the deposit (Large et al., 2000). Manganiferous dolomite alteration is measurable within the 'favourable unit' of the HYC Pyritic Shale in drill core 23 km laterally away, and perhaps further. SEDEX-associated element enrichments are also expressed as a laterally-extensive halo into the hanging wall sediments at HYC (Large et al., 2000). Through study of SEDEX host-stratigraphy in drill cores outwardly-radiating from the main deposits, Large et al., (2000) and Large and McGoldrick, (2000) developed the SEDEX Indices (Section 3.4) as a vector to mineralization.

When applied to the sections of the McDermott and Wollogorang formation analyzed in this study, the SEDEX Indices show similarities with drill cores close to HYC (Large et al., 2000). The relatively high SEDEX Metal Index values for the McDermott and Wollogorang formation lithologies are consistent with metal concentrations close to that of an orebody (Figs. 10, 11, 15). The SEDEX Metal Index considers the concentration of Zn, the limited dispersion of Pb and the widespread dispersion of Tl, with these factors increasing with proximity to an

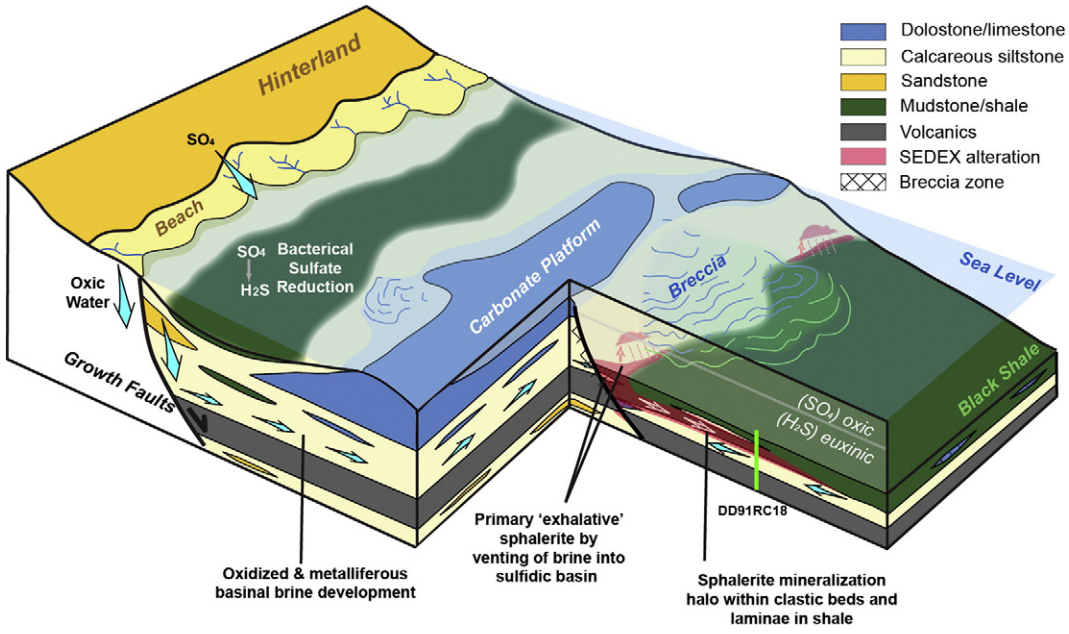


**Fig. 18.** Summary model diagram of a possible SEDEX system in Tawallah Group sediments, showing an approximate location for drill hole DD91RC18 relative to mineralization. 

orebody (Large et al., 2000; Large and McGoldrick, 2000). Metal Index factors of more than $10^4$ and $10^5$ observed in drill cores GSD7 and DD91RC18 respectively, are comparable with the favourable unit of the HYC Pyritic Shale at distances of 15 km from the main deposit (Large et al., 2000). Low MI factors in the measured sections of drill core DD91HC1 suggest that these rocks are more distal to SEDEX mineralization than those intersected in DD91RC18.

The comparison of high MI factors in rocks of the Wollogorang and McDermott formations with those at HYC assumes that dispersion mechanisms of base metals at HYC and at potential orebodies in the Tawallah Group were similar. However, the genetic model of sphalerite deposition at HYC is one of high-density metallic brines released from faults, depositing sedimentary sulfides, while lateral dispersion of dissolved Zn-Pb-Tl facilitated high metal concentrations in sediments distal to the primary site of ore deposition (Large et al., 2000). Base metals observed in the sedimentary rocks of this study include sulfides of primary authigenic sedimentary origin (e.g. Fig. 12C), and also diagenetic replacement products (e.g. Fig. 12D). The timing of these differing mineralization styles remains unknown. They may represent events by which distal synsedimentary fault zones released metallic brines into the water column and the same fluids also migrated through porous facies in the subsurface. In both scenarios, oxidized metallic brines could have been reduced by biogenic $H_2S$ in the water column or shallow sediments, or by early diagenetic/sedimentary pyrite in sediments (Fig. 18).

## 5. Conclusions

Anomalous whole rock Zn-Pb-Tl concentrations are associated with base metal sulfide mineralization and high SEDEX Indices in the studied sections of the Tawallah Group. These lithologies are therefore considered favourable for McArthur-Type SEDEX deposits. The lithological and tectonic conditions for oxidized metallic brine generation and subsequent 'exhalation' from synsedimentary faults into a reducing basin, existed during Tawallah Group times (~1.78 to ~1.73 Ga). The base metal sulfide replacement textures observed in clastic laminae within mudstones, and comparative lack of primary sphalerite are interpreted to be a distal, shallow subsurface expression of syndepositional exhalative mineralization that is suspected to have occurred in sulfidic sub-basins closer to the controlling faults.

Trace element and C/S proxies, and petrographic pyrite textures suggest there was at least intermittent euxinia in the bottom waters during the deposition of the ~1.73 Ga Wollogorang Formation rocks intersected in drill holes DD91RC18 and DD91HC1. This implies that euxinia had become established in the shallow shelf environments of the McArthur Basin by 1.73 Ga, thus providing a strongly-reducing buffer and sulfur source for potential exhaled metallic brines and subsequent primary SEDEX deposition. The studied rocks of the ~1.78 Ga McDermott Formation appear to have been deposited under anoxic but mostly sulfur-limited conditions, which may reflect the deposition in a deeper part of the basin, below the euxinic chemocline in the near-shore (Poulton et al., 2010), or that widespread euxinia had not developed in the McArthur Basin at that time.

The Wollogorang Formation, in particular, could have acted as an efficient reductant and sulfur source for metallic brines, and may be a favourable unit for SEDEX deposition. The Redbank Cu deposits, which likely represent mineralization of metals remobilized from underlying rocks such as the Wollogorang Formation, are further evidence for the mineralization potential of the Wollogorang Formation. This highlights the prospectivity for base metal mineralization in the Wollogorang Formation.

Supplementary data to this article can be found online at http://dx.doi.org/10.1016/j.oregeorev.2016.01.007.

## Acknowledgements

The authors would like to thank Michael Gazely, Robert Thorne, Monica LeGras and Claudio Delle Piane of CSIRO, and Dan Revie of the Northern Territory Geological Survey for their helpful comments and advice. Special thanks to David Cooke and Huan Li for helpful critique that greatly improved the manuscript. Armour Energy Ltd. and CSIRO Mineral Resources Discovery Programme are thanked for co-funding the study under the Researcher in Business Scheme.

## References

Ahmad, M., Dunster, J. N., and Munson, T. J. 2013. Chapter 15: McArthur Basin: in Ahmad M and Munson TJ (compilers). 'Geology and mineral resources of the Northern Territory'. Northern Territory Geological Survey, Special Publication 5.

Berner, R.A., Raiswell, R., 1983. Burial of organic carbon and pyrite sulfur in sediments over Phanerozoic time: a new theory. Geochim. Cosmochim. Acta 47 (5), 855–862.

Berner, R.A., Raiswell, R., 1984. C/S method for distinguishing freshwater from marine sedimentary rocks. Geology 12, 365–368.
Canfield, D.E., 1998. A new model for Proterozoic ocean chemistry. Nature 396, 450–453.
Canfield, D.E., 2004. The evolution of the earth surface sulfur reservoir. Am. J. Sci. 304, 839–861.
Canfield, D.E., Teske, A., 1996. Late Proterozoic rise in atmospheric oxygen concentration inferred from phylogenetic and sulfur-isotope studies. Nature 382, 127–132.
Cooke, D.R., Bull, S.W., Donovan, S., Rogers, J.R., 1998. K-metasomatism and base metal depletion in volcanic rocks from the McArthur basin, Northern Territory — implications for base metal mineralization. Econ. Geol. 93, 1237–1263.
Cooke, D.R., Bull, S.W., Large, R.R., McGoldrick, P.J., 2000. The importance of oxidized brines for the formation of some Australian Proterozoic stratiform sediment-hosted Pb–Zn (sedex) deposits. Econ. Geol. 95, 1–18.
Crusius, J., Calvert, S., Pedersen, T., Sage, D., 1996. Rhenium and molybdenum enrichments in sediments as indicators of oxic, suboxic and sulfidic conditions of deposition. Earth Planet. Sci. Lett. 145, 65–78.
Cullers, R.L., 2002. Implications of elemental concentrations for provenance, redox conditions, and metamorphic studies of shales and limestones near Pueblo, CO, USA. Chem. Geol. 191, 305–327.
Donnelly, T.H., Jackson, M.J., 1988. Sedimentology and geochemistry of a Mid-Proterozoic lacustrine unit from northern Australia. Sediment. Geol. 58, 145–169.
German, C.R., Elderfield, H., 1990. Application of the Ce anomaly as a paleoredox indicator: the ground rules. Paleoceanography 5, 823–833.
Holland, H.D., 2005. Sedimentary mineral deposits and the evolution of Earth's near-surface environments. Geology 100th Anniversary Volume Special Paper, pp. 1489–1509.
Ireland, T., Large, R.R., McGoldrick, P., Blake, M., 2004. Spatial distribution patterns of sulfur isotopes, nodular carbonate, and ore textures in the McArthur River (HYC) Zn-Pb-Ag deposit, Northern Territory, Australia. Econ. Geol. 99, 1687–1709.
Jackson, M.J., 1985. Mid-Proterozoic dolomitic varves and microcycles from the McArthur Basin, northern Australia. Sediment. Geol. 44, 301–326.
Jackson, M.J., Muir, M.D., Plumb, K.A., 1987. Geology of the southern McArthur Basin, Northern Territory. Bureau of Mineral Resources, Canberra. Bulletin 220.
Kendall, B., Creaser, R.A., Gordon, G.W., Anbar, A.D., 2009. Re–Os and Mo isotope systematics of black shales from the Middle Proterozoic Velkerri and Wollogorang Formations, McArthur Basin, northern Australia. Geochim. Cosmochim. Acta 73, 2534–2558.
Knutson, J., Ferguson, J., Roberts, W.M.B., Donnelly, T.H., Lambert, I.B., 1979. Petrogenesis of the copper-bearing breccia pipes, Redbank, Northern Territory, Australia. Econ. Geol. 74, 814–826.
Large, R.R., McGoldrick, P.J., 2000. Lithogeochemical halos and geochemical vectors to stratiform sediment hosted Zn–Pb–Ag deposits, part 1. Lady Loretta deposit, Queensland. J. Geochem. Explor. 63, 37–56.
Large, R.R., Bull, S.W., Cooke, D.R., McGoldrick, P.J., 1998. A genetic model for the HYC deposit Australia based on regional sedimentology, geochemistry and sulfide–sediment relationships. Econ. Geol. 93, 1345–1368.
Large, R.R., Bull, S.W., McGoldrick, P.J., 2000. Lithogeochemical halos and geochemical vectors to stratiform sediment hosted Zn–Pb–Ag deposits part 2. HYC deposit, McArthur River, Northern Territory. J. Geochem. Explor. 68, 105–126.
Large, R.R., Bull, S.W., McGoldrick, P.J., Walters, S., 2005. Stratiform and strata-bound Zn–Pb–Ag deposits in Proterozoic sedimentary basins, Northern Australia. Economic Geology 100th Anniversary Volume, pp. 931–963.
Leventhal, J.S., 1995. Carbon–sulfur plots top show diagenetic and epigenetic sulfidation in sediments. Geochim. Cosmochim. Acta 59, 1207–1211.
Li, H., Xi, X., 2015. Sedimentary fans: a new genetic model for sedimentary exhalative ore deposits. Ore Geol. Rev. 65, 375–389.
Lyons, T.W., Gellatly, A.M., McGoldrick, P.J., Kah, L.C., 2006. Proterozoic sedimentary exhalative (SEDEX) deposits and links to evolving global ocean chemistry. In: Kesler, S.E., Ohmoto, H. (Eds.), Evolution of Early Earth's Atmosphere, Hydrosphere, and Biosphere—Constraints from Ore Deposits. Geological Society of America Memoir 198, pp. 169–184.
Nance, W.B., Taylor, S.R., 1976. Rare earth element patterns and crustal evolution-I. Australian post Archean sedimentary rocks. Geochimica et Cosmochimica Acta 40, 1539–1551.
Page, R.W., Jackson, M.J., Krassay, A.A., 2000. Constraining sequence stratigraphy in north Australian basins: SHRIMP U–Pb zircon geochronology between Mt Isa and McArthur River. Aust. J. Earth Sci. 47, 431–459.
Parnell, J., Boyce, A.J., Mark, D., Bowden, S., Spinks, S., 2010. Nature. Early oxygenation of the terrestrial environment during the Mesoproterozoic. Nature 468, 290–293.
Piper, D.Z., Calvert, S.E., 2009. A marine biogeochemical perspective on black shale deposition. Earth-Sci. Rev. 95, 63–96.
Planavsky, N.J., McGoldrick, P., Scott, C.T., Li, C., Reinhard, C.T., Kelly, A.E., Chu, X., Bekker, A., Love, G.D., Lyons, T.W., 2011. Widespread iron-rich conditions in the mid-Proterozoic ocean. Nature 477, 448–452.
Plumb, K.A., 1979. The tectonic evolution of Australia. Earth-Sci. Rev. 14, 205–249.
Poulton, S.W., Fralick, P.W., Canfield, D.E., 2010. Spatial variability in oceanic redox structure 1.8 billion years ago. Nat. Geosci. 3, 486–490.
Rawlings, D.J., 1999. Stratigraphic resolution of a multiphase intracratonic basin system: the McArthur Basin, northern Australia. Aust. J. Earth Sci. 46, 703–723.
Redbank Copper Ltd, 2010. Redbank Development Study. http://www.redbankcopper.com.au/images/development_study_may2010.pdf, accessed 15 January 2016.
Rod, E., 1978. Decollement folds in Redbank area, Northern Territory. J. Geol. Soc. Aust. 25, 89–95.
Ross, J.D.K., Bustin, R.M., 2009. Investigating the use of sedimentary geochemical proxies for paleoenvironment interpretation of thermally mature organic-rich strata: examples from the Devonian–Mississippian shales, Western Canadian Sedimentary Basin. Chem. Geol. 260, 1–19.
Shen, Y., Canfield, D.E., Knoll, A.H., 2002. Middle Proterozoic ocean chemistry: evidence from the McArthur Basin, Northern Australia. Am. J. Sci. 302, 81–109.
Slack, J.F., Grenne, T., Bekker, A., Rouxel, O.J., Lindberg, P.A., 2007. Suboxic deep seawater in the late Paleoproterozoic: evidence from hematitic chert and iron formation related to seafloor-hydrothermal sulfide deposits, central Arizona, USA. Earth Planet. Sci. Lett. 255, 243–256.
Stanley, C.R., Lawie, D., 2007. Average relative error in geochemical determinations: classification, calculation, and a plea for consistency. Min. Explor. Geology 16, 267–275.
Strauss, H., 1993. The sulfur isotopic record of Precambrian sulfates: new data and a critical evaluation of the existing record. Precambrian Res. 63, 225–246.
Xu, G., Hannah, J.L., Bingen, B., Georgiev, S., Stein, H.J., 2012. Digestion methods for trace element measurements in shales: Paleoredox proxies examined. Chem. Geol. 324-325, 132–147.